AD-A061 031 ARMY MILITARY PERSONNEL CENTER ALEXANDRIA VA F/G 20/8
A SEARCH FOR EVAPORATION RESIDUES IN REACTIONS OF CHLORINE ON T--ETC(U)
AUG 78 D F GROGAN

UNCLASSIFIED NL

1 OF 1
AD
A061 031

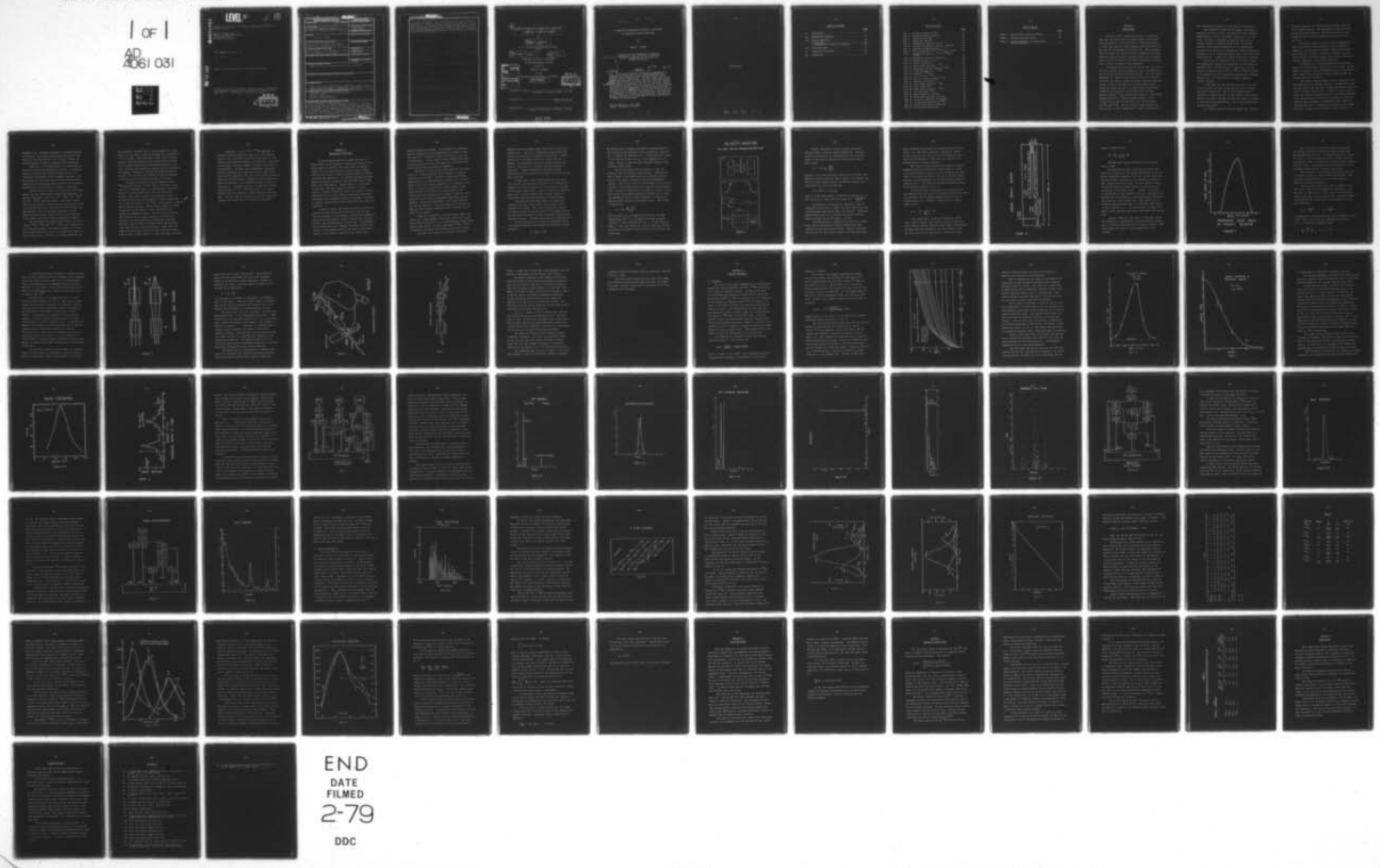

END
DATE
FILMED
2-79
DDC

LEVEL II

2

A Search for Evaporation Residues in Reactions of Chlorine on Thulium and Gold

Daniel F Grogan, CPT
HQDA, MILPERCEN (DAPC-OPP-E)
200 Stovall Street
Alexandria, VA 22332

Final report, August 1978

391 191

A thesis submitted to the Massachusetts Institute of Technology, Cambridge, Massachusetts, in partial fulfillment of the requirements for the degree of Master of Science.

SECURITY CLASSIFICATION OF THIS PAGE (When Data Entered) UNCLASSIFIED

REPORT DOCUMENTATION PAGE	READ INSTRUCTIONS BEFORE COMPLETING FORM
1. REPORT NUMBER / 2. GOVT ACCESSION NO.	3. RECIPIENT'S CATALOG NUMBER
4. TITLE (and Subtitle) A Search for Evaporation Residues in Reactions of Chlorine on Thulium and Gold	5. TYPE OF REPORT & PERIOD COVERED Final Report August 1978 6. PERFORMING ORG. REPORT NUMBER
7. AUTHOR(s) Daniel F Grogan	8. CONTRACT OR GRANT NUMBER(s)
9. PERFORMING ORGANIZATION NAME AND ADDRESS Student, HQDA, MILPERCEN (DAPC-OPP-E) 200 Stovall St, Alexandria, Va 22332	10. PROGRAM ELEMENT, PROJECT, TASK AREA & WORK UNIT NUMBERS
11. CONTROLLING OFFICE NAME AND ADDRESS HQDA, MILPERCEN, ATTN: DAPC-OPP-E, 200 Stovall St, Alexandria, VA 22332	12. REPORT DATE August 1978 13. NUMBER OF PAGES 81
14. MONITORING AGENCY NAME & ADDRESS(if different from Controlling Office)	15. SECURITY CLASS. (of this report) U 15a. DECLASSIFICATION/DOWNGRADING SCHEDULE

16. DISTRIBUTION STATEMENT (of this Report)

Approved for public release; distribution unlimited.

17. DISTRIBUTION STATEMENT (of the abstract entered in Block 20, if different from Report)

18. SUPPLEMENTARY NOTES

Report is an experimental thesis submitted in partial fulfillment of the requirements for Master of Science Degree at the Massachusetts Institute of Technology, August 1978

19. KEY WORDS (Continue on reverse side if necessary and identify by block number)

Evaporation residues of fusion reactions
Heavy ion fusion
Chlorine + Gold Reaction
Chlorine + Thulium Reaction

20. ABSTRACT (Continue on reverse side if necessary and identify by block number)

Recoiling evaporation residues from the fusion of ^{37}Cl and two proton rich nuclei, ^{169}Tm and ^{197}Au, were studied at lab energies of 151 through 186 MeV, and 176 through 184 MeV, respectively. The zero degree excitation function was measured for the Tm reaction (compound nucleus ^{206}Rn) and was found to peak at 156, 167, 177, and 182 MeV corresponding to emission of 3n, 4n, 5n, and 4n-1p, respectively, with a maximum total cross section of 1.09 millibarns,

DD FORM 1 JAN 73 1473 EDITION OF 1 NOV 65 IS OBSOLETE

UNCLASSIFIED
SECURITY CLASSIFICATION OF THIS PAGE (When Data Entered)

20

occurring at 166 MeV. A half life determination was made from alpha decay of ^{202}Rn and it was found to be 10.5±.9 sec. An upper limit for the fusion reaction ^{37}Cl+^{197}Au was put at 60 nanobarns at 179 MeV. The experimental work employed the MIT Heavy Ion Group's upgraded apparatus at Brookhaven National Laboratory, the principles, testing, and operation of which are detailed here.

(6) A SEARCH FOR EVAPORATION RESIDUES IN REACTIONS OF CHLORINE ON THULIUM AND GOLD

by

(10) DANIEL F. GROGAN

B.S., United States Military Academy
(1972)

(9) Final repts (12) 85 p.

SUBMITTED IN PARTIAL FULFILLMENT

OF THE REQUIREMENTS FOR THE

DEGREE OF

MASTER OF SCIENCE

at the

MASSACHUSETTS INSTITUTE OF TECHNOLOGY

(11) August 1978

Signature of Author.....
Department of Physics, August 25, 1978

Certified by.....
Thesis Supervisor

Accepted by.....
Chairman, Departmental Committee on Theses

391 497

A SEARCH FOR EVAPORATION RESIDUES IN REACTIONS OF CHLORINE ON THULIUM AND GOLD

by

DANIEL F. GROGAN

Submitted to the Department of Physics
on August 25, 1978, in partial fulfillment
of the requirements for the degree of
Master of Science

ABSTRACT

Recoiling evaporation residues from the fusion of ^{37}Cl and two proton rich nuclei, ^{169}Tm and ^{197}Au, were studied at lab energies of 151 through 186 MeV, and 176 through 184 MeV, respectively. The zero degree excitation function was measured for the Tm reaction (compound nucleus ^{206}Rn) and was found to peak at 156, 167, 177, and 182 MeV corresponding to emission of 3n, 4n, 5n, and 4n-1p, respectively, with a maximum total cross section of 1.09 millibarns, occurring at 166 MeV. A half life determination was made from alpha decay of ^{202}Rn and it was found to be 10.5±.9 sec. An upper limit for the fusion reaction ^{37}Cl + ^{197}Au was put at 60 nanobarns at 179 MeV. The experimental work employed the MIT Heavy Ion Group's upgraded apparatus at Brookhaven National Laboratory, the principles, testing, and operation of which are detailed here.

Thesis Supervisor: H.A. Enge
Title: Professor of Physics

To my mother

TABLE OF CONTENTS

		Page
I.	Introduction	7
II.	Experimental Apparatus	13
III.	Thulium Experiment	31
	A. Procedure	31
	B. Experimental Results and Analysis	55
IV.	Gold Experiment	73
V.	Comparison With Theory	75
VI.	Conclusions	78

LIST OF FIGURES

		Page
Fig. 1	Velocity selector fields	17
Fig. 2	Modified velocity selector	20
Fig. 3	Solid angle vs. $\frac{\Delta v}{v}$	22
Fig. 4	Quadrupole focusing	25
Fig. 5	Experimental apparatus system	27
Fig. 6	Particle trajectories through apparatus	28
Fig. 7	Equilibrium charge states	33
Fig. 8	Velocity profile: $^{37}Cl + ^{169}Tm$ at 175 MeV	35
Fig. 9	Angular distribution: $^{37}Cl + ^{169}Tm$ at 175 MeV	36
Fig. 10	Quadrupole focusing optimization	38
Fig. 11	Residue tracks in lexan	39
Fig. 12	Initial electronics	41
Fig. 13	Total energy spectrum: ^{169}Tm	43
Fig. 14	Evaporation residue spectrum: ^{169}Tm	44
Fig. 15	Out-of-beam spectrum: ^{169}Tm	45
Fig. 16	Elastics: ^{169}Tm	46
Fig. 17	Time spectrum: ^{169}Tm	47
Fig. 18	Time vs. energy spectrum: ^{169}Tm	48
Fig. 19	Improved electronics	49
Fig. 20	Total energy spectrum: ^{169}Tm	51
Fig. 21	Final electronics	53
Fig. 22	Total energy spectrum: ^{169}Tm	54
Fig. 23	Time spectrum: ^{202}Rn	56
Fig. 24	Decay schemes of nuclides	58
Fig. 25	Excitation functions of parents	60
Fig. 26	Excitation functions of daughters	61
Fig. 27	Lifetime determination of ^{202}Rn	62
Fig. 28	Parents and adjusted daughters	67
Fig. 29	Fusion gates and parents	69

LIST OF TABLES

		Page
Table 1	Recoil nuclei ionizing energies	64
Table 2	Accepted branching ratios	65
Table 3	Relative Abundance of Fusion Evaporation Residues	77

CHAPTER I

INTRODUCTION

The early 1940's heralded the advent of a new scientific age, one marked by an increased concern with exploration and discovery. During this age, of which the present is a part, the number of known elements increased from 92 to 106, and that of nuclides from 300 to 1500. These nuclides form a peninsula on a chart of Z vs N, unstable at its edges against β decay and electron capture, and at its tip against alpha emission and fission, the latter instability resulting from a greatly increased Coulomb repulsion.

In keeping with the spirit of the new age, much effort has been expended toward extending the tip of the peninsula, but as yet few successes have been enjoyed. Still the effort continues, for nuclear theory predicts that at a Z of about 114 exists an island of stability against the above mentioned decays -- this is the region of the superheavies, whose stability results from the increased binding energy associated with the closing of a proton shell due to single particle orbits.[1] This stabilizing effect, it is predicted, should extend over a range of neutron numbers, as the reverse case is seen to hold true, as in the N=126 shell of ^{214}Ac and ^{215}Th. The half lives of these nuclides are 8.2 sec and 1.2 sec, respectively.[2] It is on this region

that the greatest proportion of attention is now focused.

That attention is based on the appeal of discovery, certainly, but only in part. The quest for a more complete understanding of nature also forms a great portion of that basis. A number of contemporary theories which provide similar results for currently known nuclei would yield different results when extrapolated to the superheavies. And there is no certainty in denying that hitherto unobserved phenomena, with yet unrealized applications, will result from their discovery. Indeed, this search is certainly justified.

Efforts in the search have taken the form of laboratory experiments involving the formation of nearly spherical compound nuclei via the fusion of a projectile with its target, an example being the $^{48}Ca + {}^{248}Cm \rightarrow {}^{296}116^{*}$ reaction. It is expected that this compound nucleus will most probably fission, but it may also deexcite by alpha, gamma, or neutron emission.

It has been seen that the cross section for the production of heavy nuclides is greatest for large Z targets, and small Z projectiles. But it is not known whether spherical or deformed nuclei are best suited in the production of cold nuclei, the case in which the endoergic Q value is less than the Coulomb barrier. Here, fission competition would be minimized.[1)]

If a heavy projectile is used, perhaps only a portion

of that projectile will combine with the target resulting in a transfer reaction. The remainder will then carry off energy and angular momentum. The practicability of this method suffers from unfortunately minute reaction cross sections.

Yet another scheme of attack is that of bombarding a heavy target with a heavy projectile, such as uranium on uranium, in the hope that the massive nucleus will fission and produce as a product a superheavy. However, it is believed by many that these products will be quite elongated, and will themselves fission before detection.

A renewed hope is being generated with the development of new accelerators, such as that of Oak Ridge, and the UNILAC in Germany. These new machines have been designed for more intense beams and greater energy resolution than previously have been available.

The repeated lack of success clearly indicates a lack of understanding of processes involved. Perhaps coalescence does not occur under some energy threshold, and the nucleus must form in a highly excited state. Perhaps, for heavy projectiles, the concept of Coulomb barrier is in need of modification, since distortion calculations in heavy ion reactions show increased oblateness of projectiles, which result in increased barriers.[3] Perhaps an alternative to the liquid drop model, which fails to account for the resistance to

deformation for permanently deformed or spherical nuclei, is indicated. But theory modifications must reflect the results of good experiments. And, to date, the most auspicious technique is that of compound nucleus formation.

These gaps in the understanding of the processes involved in creating the superheavies will not, it should be clear, be filled by any means other than by that of an incremental, deliberate, and developmental approach. Only by starting with reactions which are well understood and progressing to increasingly massive systems will insight be developed into the mechanisms of superheavy formation.

The MIT Heavy Ion Group of the Laboratory for Nuclear Science has been aggressively pursuing this stratagem. As part of its program, reactions of $^{32}S + ^{58}Ni$, $^{32}S + ^{70}Ge$,[4] and $^{32}S + ^{112}Sn$[5] have been studied. Selection of these reactions was based on evidence that if the superheavies are to be created via fusion, they will have to be proton rich. Consequently, in all of the above reactions, the most neutron deficient stable isotope was used for targets to create proton rich, beta unstable evaporation residues.

The experiments described in this thesis, the reactions of $^{37}Cl + ^{169}Tm$, and $^{37}Cl + ^{197}Au$, are a continuation of the Group's program. The primary interest was in the more massive gold system; but as it is well known that its fusion cross section is minute, the thulium system was to

have provided a thorough test of the new apparatus in preparation for the gold, as well as providing some information in its own right. With convincing results that the equipment was functioning properly with thulium, work was begun on gold, which provided only a questionable degree of success. Attention was returned to thulium, and the experiment was expanded. Though this reflects the actual conduct of the work, for continuity the thulium run will be described in its entirety, to be followed by that of the gold.

The ground state Q value of the compound nucleus ^{206}Rn formed by fusing ^{37}Cl and ^{169}Tm is -84.4 MeV, resulting, for the energies used, in a representative excitation energy of 51.8 MeV, which would leave the evaporation residues fairly close in mass to the compound nucleus. It is expected that the high likelihood of fission would leave only a small percentage of the ^{206}Rn to form products, primarily through nucleon emission. These residues should be readily recognizable by the energy of their associated alpha particles in subsequent decays. The low velocity evaporation residues will be emitted primarily in the forward direction, the distribution being broadened by multiple scattering effects within the target and by particle emission, requiring zero degree observation. Also, since the cross section is known to be very small, focusing of these products onto a single detector is also very highly desirable.

Preliminary work on a $^{35}Cl + ^{169}Tm$ experiment at Brookhaven National Laboratory made use of the velocity selector (to be described in greater detail later) of the group's Energy Mass Spectrometer, and indicated a clear need to ameliorate existing equipment if useful results were to be forthcoming. In these early experiments, evaporation residue measurements were made using barrier type solid state detectors mounted at the exit of the velocity selector. Difficulty resulted from the swamping of these detectors by beam tail particles of the selected velocity at angles of less than 2°. It became clear that as audacious an undertaking as that of $^{37}Cl + ^{197}Au$ would have to be held in abeyance until modifications to reduce this beam tail were made. The work, however, did propose a total evaporation residue cross section of 267 microbarns at 170 MeV.[6)]

CHAPTER II

EXPERIMENTAL APPARATUS

As the considered heavy ion fusion reactions are characterized by the emission of evaporation residues with a small angular distribution and a low yield, an apparatus capable of zero degree operation without adverse effects from the beam as well as spacial focusing would be required to perform the experiments. An upgraded apparatus has been added to the Heavy Ion group's system at BNL to meet these operational requirements. Ideally suited for experiments of this type, its major components include a velocity selector, a magnetic quadrupole pair, and a magnetic dipole. Mounted directly onto the existing recoil mass spectrometer arrangement, this equipment affords an increased flexibility in reaction studies such as those about which this thesis is concerned.

In general terms, the velocity selector discriminates against particles emitted from the target based on their velocity by means of an arrangement of mutually perpendicular electrostatic and magnetic fields, resulting in a vertical velocity analyzed spectrum at its exit port. The quadrupole pair's fields then effect stigmatic focusing of these particles. If the dipole element is not used, a solid state detector in the dipole's "velocity port" collects the

focused evaporation residues. If the dipole is energized, then the particles are bent downward by its fields through the "mass port" to produce a spectrum analyzed by its mass to charge ratio. In this mode of recoil isotope separation, a position sensitive solid state detector, or nuclear track plates, may be used to collect the spectra.

The source of beam is BNL's MP-7 tandem Van de Graaff generator, recently upgraded and now capable of terminal voltages of up to 14 MV. The beam is shaped and focused magnetically as it proceeds along the beam line. A collimator is the first element encountered. It consists of two sets of apertures separated by a 20-inch length of pipe. These apertures are mounted on rotating drums so that differently sized openings may be selected. They are lined with gold foil to eliminate possible undesirable reaction products. During the experiments, a 0.375-inch diameter aperture was selected. Electrical connections are made so that any beam particles impinging on the collimator may be monitored as current.

Targets are mounted on a vertical target ladder, and housed in a target chamber. The ladder affords up to four target frame mountings, so as to allow changing targets without breaking vacuum. In these experiments, ^{169}Tm, ^{197}Au, Sn (natural) and quartz (for beam focusing) were mounted.

One half inch in front of the target ladder are

arranged four spectroscopy grade carbon rods to form a rectangular slit. Each rod is independently adjustable, and current from each may be independently monitored. Optimal collimation is determined when these currents are at a minimum. The dimensions of the slit during the runs were 0.055 in. and 0.150 in., vertically and horizontally, respectively. A small incandescent lamp allows visual inspection of target condition; the lamp is turned off during data collection.

An upper and a lower 25 mm^2 surface barrier solid state detector are installed at angles of 30.3° and 28.4°, respectively, and at distances of 14.4 cm and 14.5 cm from the beam spot on the target. Each is masked by an aluminum plate with a 0.21 cm diameter hole to allow passage of elastically scattered beam particles for normalization.

Emerging from the target chamber the evaporation residues enter into a Wien filter, which analyzes them according to velocity. This so-called velocity selector has been described in the literature,[7,8] although the need for zero degree operation in these experiments necessitated some modifications. The basic principles are outlined below.

A charged particle of velocity $\vec{v}$ experiences forces in an electromagnetic field given by the well-known Lorentz equation:

$$\vec{F} = q(\vec{E} + \vec{v} \times \vec{B})$$

By appropriately arranging the fields to be perpendicular to the velocity of the particle as well as mutually, the force on -- and hence the deflection of -- the particle will vanish if its velocity is such that $v_o = E/B$, regardless of its charge. Implied is that the above condition holds for the fringing fields as well.

But the fringing fields are seldom, if ever, so amenable, and thus introduce complications. Since the air gap is larger in the magnet than in the electrostatic deflector, the latter's fringing field is correspondingly narrower. The overall result at the entrance of the velocity selector is that the particle first experiences the magnetic force, by which it is deflected, and then the electric force. The electric force does straighten the orbit, but not without imposing an offset in the trajectory. An identically opposite offset results at the device's exit. This offset is expressed by

$$\Delta x = I\, Bq\, \frac{D_m^2 - D_E^2}{m\, v_o}$$

where D_m and D_E are the magnetic and electric air gaps, respectively, and I is a fringing field shape dependent integral.[9] This is depicted in fig. 1. In the device at hand, I = 0.85, D_m = 10 cm, D_E = 2.54 cm, Bq/m v_o = 169 cm, resulting in a required vertical offset of 0.47 cm from the target spot.

VELOCITY SELECTOR

From Enge, Nucl. Inst. & Methods 145 (1977) 280

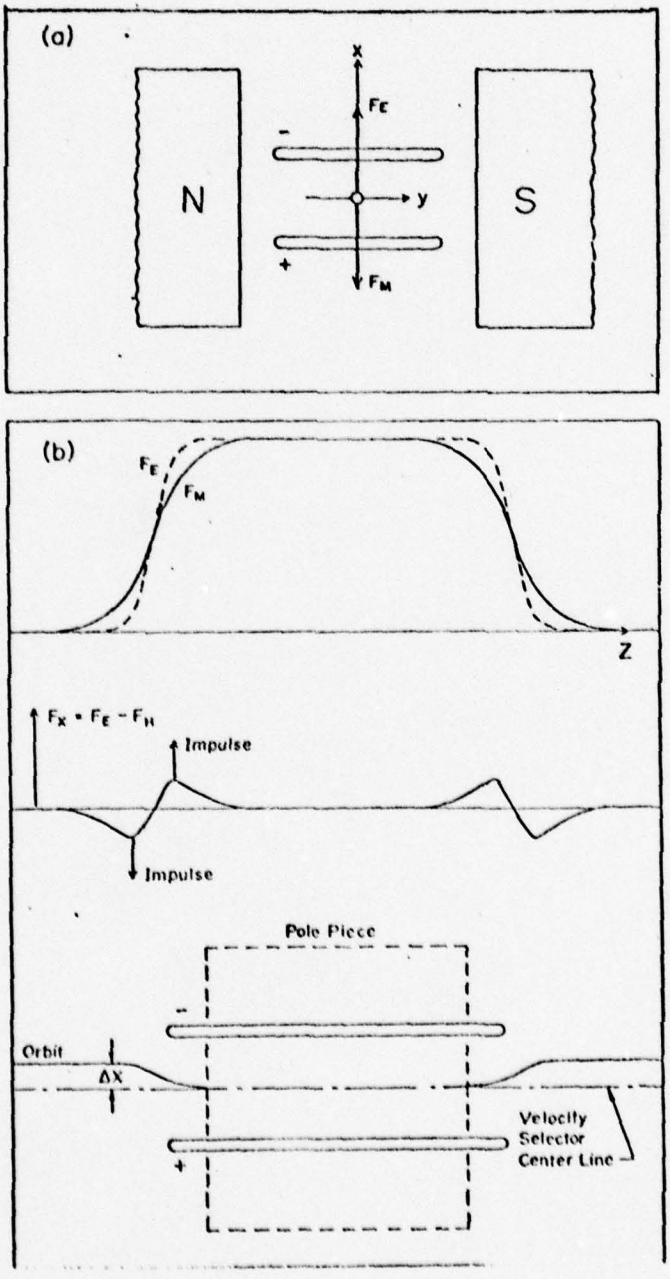

figure 1

Another complication of the ill-behaved magnetic fringing fields is that of vertical defocusing. Assuming perfect field overlap, the condition may be represented by lenses at the entrance and exit of the fringing field of focal length

$$1/f = -0.07\ D_m\ \frac{B^2q^2}{m^2v_o^2}$$

Applying a thin lens condition to the velocity selector (the effective field is much less than $m\ v_o/Bq$), and including the effects of the fringing fields, the velocity selector may be represented by a thin lens such that

$$1/f = B^2q^2\ (L - 0.14\ D_m)$$

where L is the field length. A particle of velocity $v_o + \Delta v$ will emerge at $x = -\frac{1}{2}\ \theta L$ and at an angle of $\theta = \frac{-L\Delta v\ Bq}{v_o^2\ m}$. 9)

The apparatus is designed for achieving a velocity resolution of the order of 1/500. For this, high fields and correspondingly small solid angles are required. Fields are about 40 kV/cm and 4 kG to separate the fusion products, whose velocities are of the order of 10^7 m/s.

The beam particles' velocities are from 2 to 4 times this, and for the most part they are stopped when they collide with the electrostatic plates. However, particles in the beam tail have smaller energies, and correspondingly

lower velocities which allow their passage through the ExB filter. For zero degree operation, required for fusion product detection, the separation of the evaporation residues from the profusion of beam particles emitted in the forward direction becomes essential.

The original design included four beryllium covered aluminum baffles on the positive (lower) plate as a beam trap, proportionately sized so as not to decrease the solid angle for the particles with a velocity of interest; these, however, proved ineffectual, as the detector was swamped by unwanted counts. The condition has been corrected by means of the solution depicted in fig. 2.

A portion of the electrostatic field plates was cut and separated from the rest of the velocity selector, so that ions emerging from the target chamber would first be deflected upward, as a function of their charge to energy ratio, since:

$$\Delta x_E \propto \frac{l}{\rho_\varepsilon} \propto \frac{l}{\frac{mv^2}{q}\frac{1}{\varepsilon}} \propto \frac{q}{E}$$

This electrostatic field was followed by a drift space (with no fields), and then by a region of pure magnetic field of the same effective field length and producing the same radius of curvature as the electrostatic field. Thus particles are bent downward as a function of their

FIGURE 2

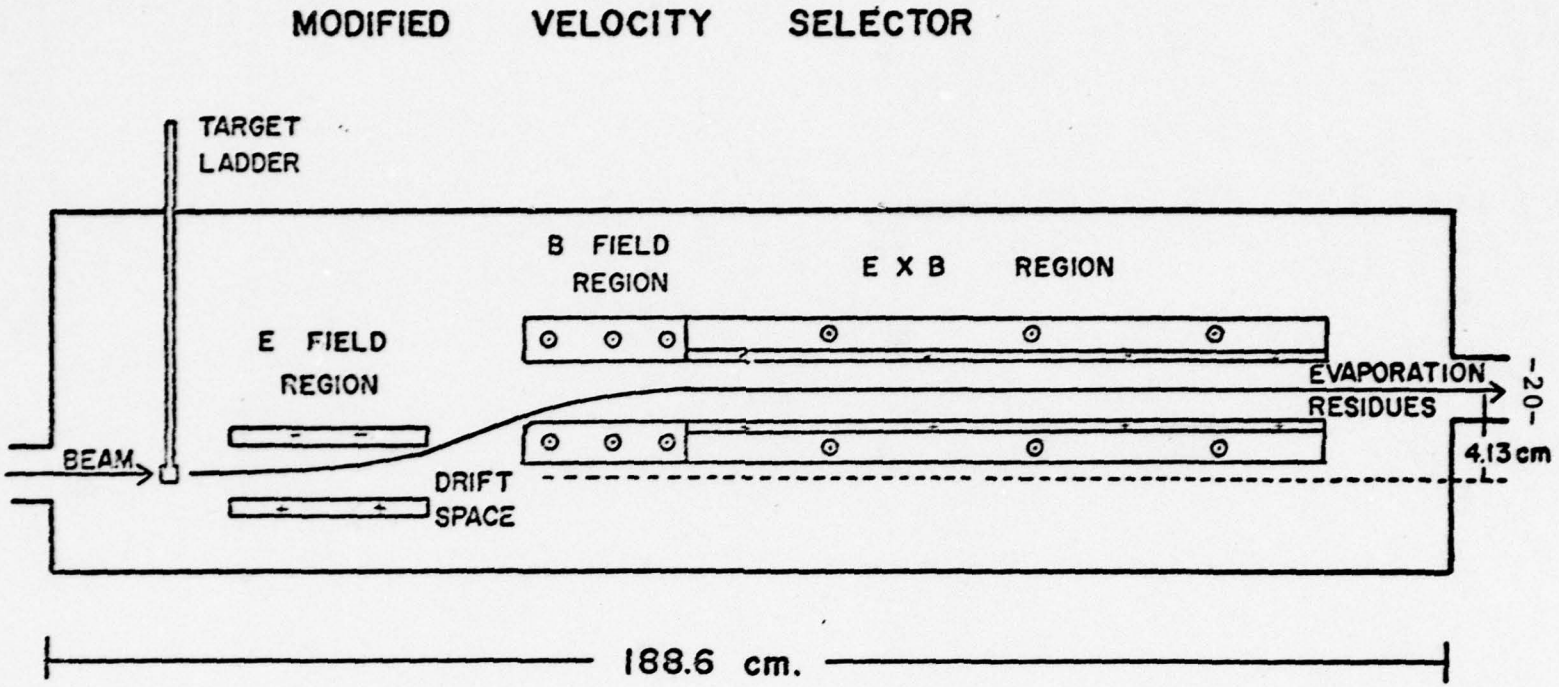
MODIFIED VELOCITY SELECTOR
TARGET LADDER
B FIELD REGION
E X B REGION
E FIELD REGION
EVAPORATION RESIDUES
-20-
4.13 cm
BEAM
DRIFT SPACE
188.6 cm.

charge to momentum ratio,

$$\Delta x_B \propto \frac{1}{\rho_B} \propto \frac{1}{\frac{p}{q} \times \frac{1}{B}} \propto \frac{q}{p}$$

The $\vec{E}x\vec{B}$ region follows, selecting velocities such that $v_o = E/B$.

The separation of pure E and pure B fields by the drift space results in a net upward displacement of the slow moving evaporation residues of 4.13 cm. By this amount the velocity selector (exclusive of the separate E field) has been elevated above the target. The more energetic beam is now removed from the residues since it is deflected much less by the electrostatic field. Instead, it impinges on the Faraday cup and registers a current. That portion of the beam tail with velocity v_o which would allow it through the filter has a much smaller mass, hence energy, and is deflected proportionately more. An adjustable upper baffle is set to interdict it. It is clear that the higher the fields, while retaining their ratio, the smaller the velocity bite.

Figure 3 shows the solid angle of acceptance versus the deviation of velocity from v_o for the velocity selector, for ρ = 169 cm, as determined by the Raytrace program. This relationship will serve in the determination of cross sections.

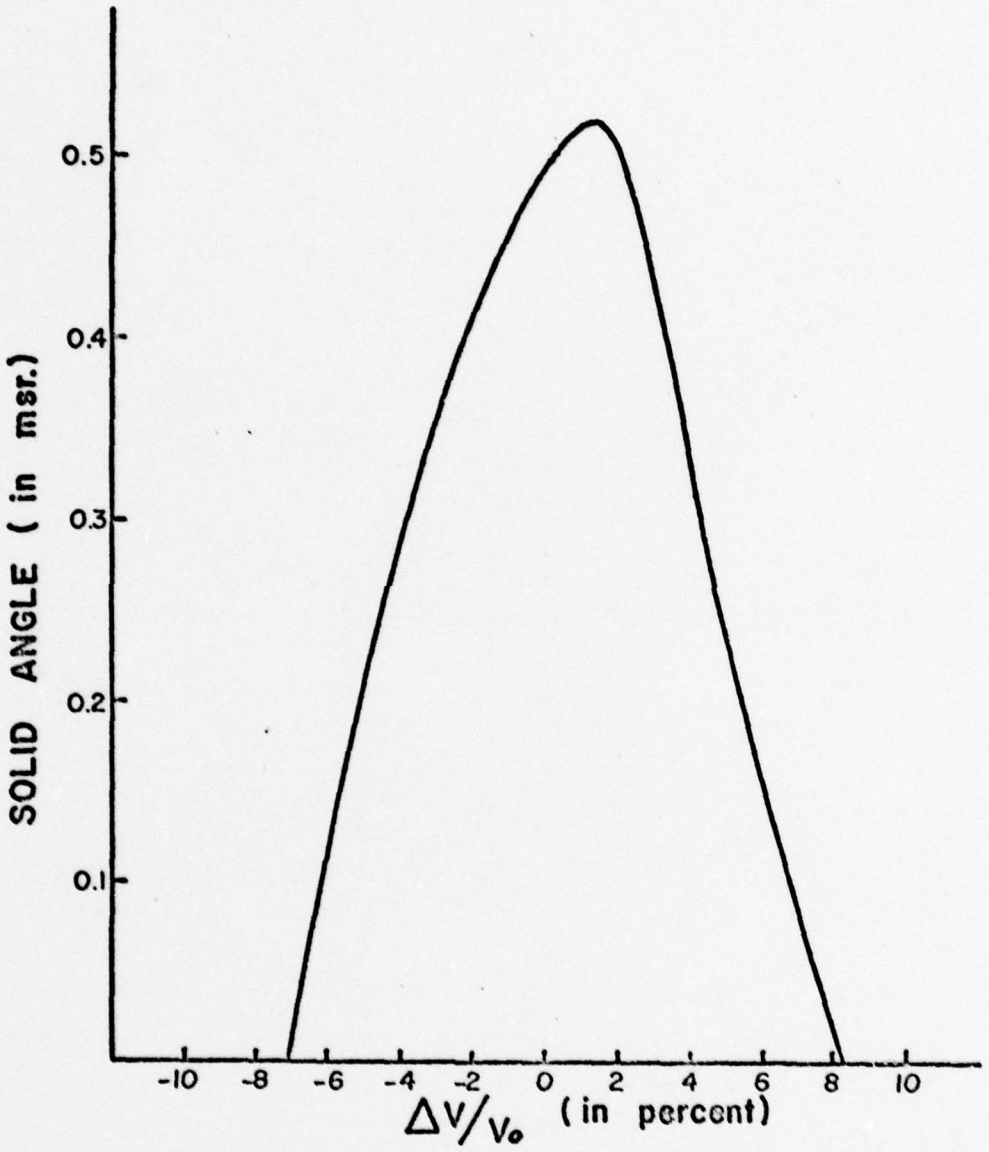

ACCEPTANCE SOLID ANGLE
OF VELOCITY SELECTOR

FIGURE 3

The electrostatic plates are supplied by Spellman High Voltage Electronics Corporation model RHR 60P30/RVL and RHR 60H30/RVL ($\pm$60 kV). The voltage difference between the plates is remotely monitored using a digital voltmeter. The magnetic fields are supplied by an Alpha (Donner Systron) 440 volt supply. A permanently mounted digital Hall effect gaussmeter enables remote readings of the fields.

The desirability for focusing the emerging particles for enhancing count rate has already been discussed. The focusing is accomplished by a pair of Spectromagnetic Industries magnetic quadrupoles.

This focusing ability stems from the nature of the quad field. For a quad with parabolic pole pieces, it is true that $B_x = \frac{B_o}{R} y$ and $B_y = \frac{B_o}{R} x$, with R as the aperture radius and B_o the field at the pole tip. Positively charged ions moving in the +Z direction, by the Lorentz force law, will experience

$$F_x = -\frac{v B_o x}{R} \quad ; \quad F_y = +\frac{v B_o y}{R} ,$$

a focusing force in the $\hat{x}$ direction, and a defocusing one in the $\hat{y}$. Then, with a thin lens approximation, valid for $f_o >> \ell$, ℓ being the effective length

$$\frac{1}{f_o} = \frac{B_o}{R} \frac{\ell}{B\rho} , \quad f_x = f_o = -f_y$$

If two such quadrupoles are used as a system, then one will act like a converging lens in one plane, and a diverging lens in the other; the other quad will be exactly opposite. Since the deflection of a ray through a thin lens is proportional to the distance of that ray from the optical axis, the pair of quadrupoles gives focusing in both directions, as shown in fig. 4.[10)]

The pole pieces in the quads used are 8 in. long, with an aperture diameter of 4.125 in. The coils are water cooled, and each quad is protected by a McDonnell Corporation flow switch wired to the power supply. The supply is the same used for the magnetic fields of the velocity selector. No guassmeter is employed for field strength readings. Instead, optimal focusing has been determined experimentally, as will be described later. As indicated by Raytrace, the field ratio of the downstream quad to the upstream is set at 1.063 using resistors in a current-dividing circuit. This ratio is used only if the dipole is not incorporated in the system. If it is, that ratio is set of 1.085, to take into account the small focusing of the dipole. A toggle switch enables selection of the appropriate field ratio.

The last major component of the system is a magnetic dipole. If the dipole is not energized, then the residues would be focused onto a solid state detector at the calcu-

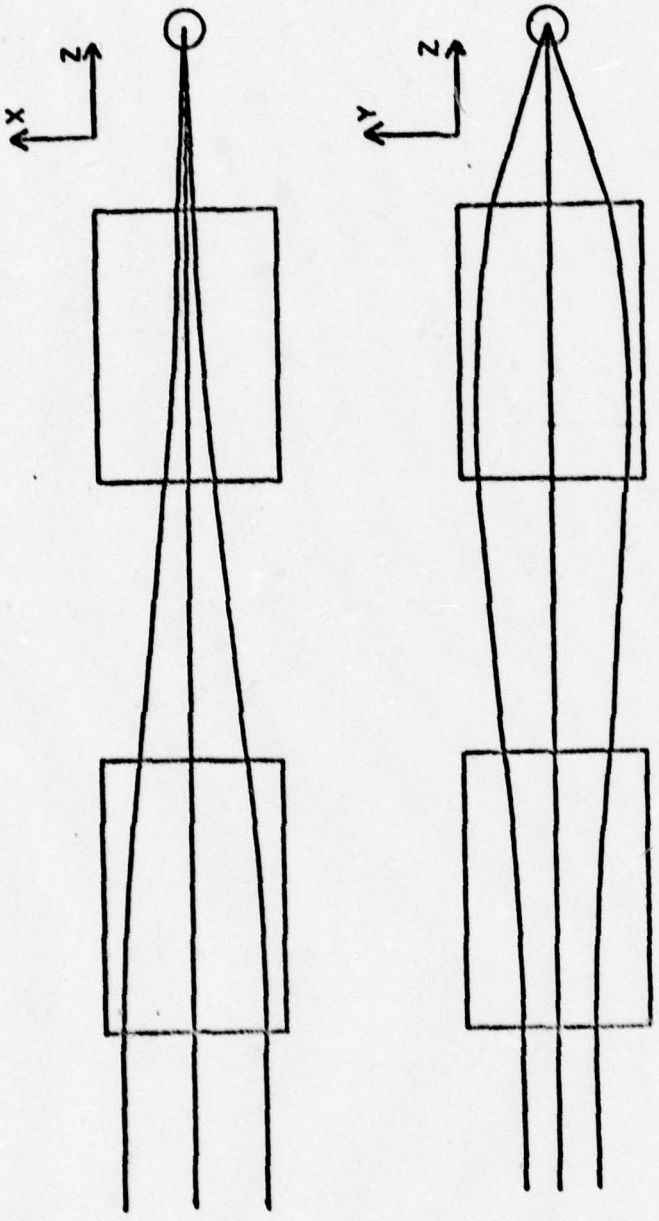

QUADRUPOLE PAIR FOCUSING

FIGURE 4

lated focal point in the velocity port. Integrating the dipole into the system makes full use of the analyzing capability of the recoil isotope separator; isotopes are separated vertically. Since the magnetic rigidity for an ion beam can be expressed as

$$B\rho = p/q = \frac{m}{q} v ,$$

ρ is the radius of curvature of the orbit; p is momentum, and q is the charge. Thus, for a given velocity (as determined by the velocity selector) and a given B (set on the dipole), the displacement is seen proportional to m/q.

The pole pieces are 12 in. in length. The dipole was manufactured with a 1 in. airgap between pole pieces. With steel spacers this has been increased to 1.5 in. to accommodate a specially designed vacuum chamber. That chamber is depicted in figure 6. The upper or "velocity port" is without isotope separation; the lower or "mass port" separates isotopes. The focal plane for the mass port lies at an angle of about 5° to the particle trajectories, as determined by Raytrace. The angular deflection of 12.6° of the mass port was also determined by Raytrace to eliminate the velocity dispersion of the velocity selector.

The dipole circuit is protected by a McDonell flow switch in conjunction with the coil water cooling system. Two Hewlett-Packard 6269B DC power supplies supply the

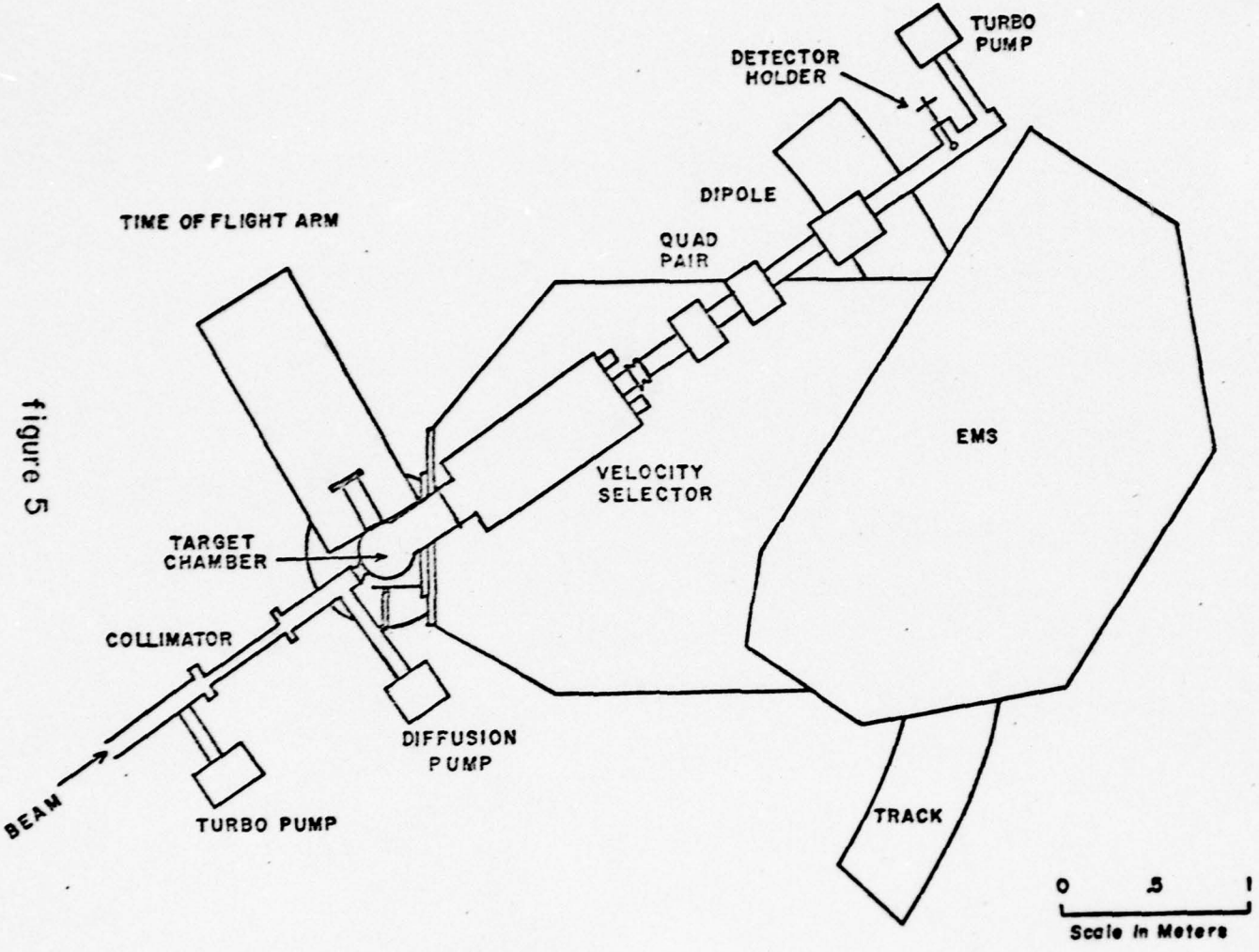

figure 5

EXPERIMENTAL APPARATUS

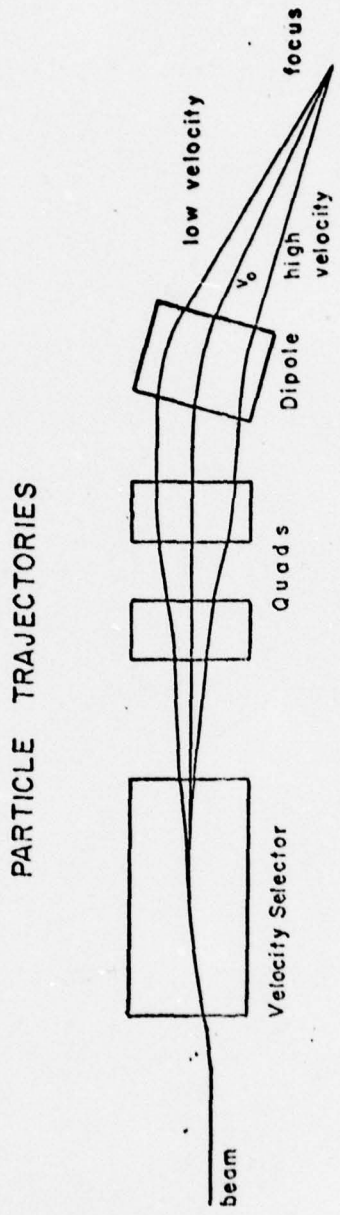
PARTICLE TRAJECTORIES
low velocity
focus
v_o
high velocity
Dipole
Quads
Velocity Selector
beam

figure 6

dipole. A probe for an Alpha model 3104 gaussmeter has been affixed to the chamber for consistent field readings.

The physical mounting of the hardware necessitated some modification to the existing arrangement of apparatus. Even with the velocity selector at its fullest deflection there was insufficient space between it on the split pole magnet of the EMS to mount the 210 cm long assembly. Since a vertical step on the mounting platform precluded any further deflection of the velocity filter stand, the mounting of the selector on the stand was altered. The resulting increased angular deflection of the stand allowed sufficient room to mount the apparatus.

Two 4 in. I beams, 72 in. in length, were bolted to the platform to form a track upon which a half inch steel plate is laid. An angle iron structure rests on the plate, the structure supported by three adjustable leveling pods, so that fine vertical adjustments and leveling are possible. On this structure are mounted the quads and dipole.

The quads sit directly on the framework, with no mechanical attachment. The dipole is supported by three of the same type pods that support the angle framework. Steel ears have been welded at an angle so the natural position for the dipole is at a 6.3° cant to the beam line.

The quadrupole pair has a 31 in. piece of 4 in. beam pipe through it, which is permanently mounted, a standard

Brookhaven flange having been welded with the pipe installed through the quads.

The vacuum system comprises three floor turbo pumps, two of which are trapped with liquid nitrogen, and a diffusion pump. Vacuums achieved were of the order of 10^{-6} torr throughout the experiments.

CHAPTER III

THULIUM EXPERIMENT

A. Procedure

As a test of the proper functioning of the apparatus, evaporation residues produced from $^{37}Cl + ^{169}Tm$ were studied over a range of incident energies. Included among these were some below the theoretical Coulomb barrier of 163 MeV in the lab frame[11] to check the validity of this prediction. If one assumes the compound nucleus ^{206}Rn is formed in the center of the target thickness, and includes energy degradation of the beam in his consideration, he finds that the pre-evaporation energy is about 31 MeV, for a 350 microgram/cm^2 target of ^{169}Tm and a 175 MeV ^{37}Cl beam. And if he further divines that characteristically four neutrons will be emitted isotropically without a change in velocity of the residue, but that its energy is degraded by the target, then energy will drop to about 30 MeV. Thus initial efforts were toward a product of corresponding velocity and mass.

To determine the required B field of the velocity selector knowing $B\rho = p/q$, one may use

$$B(kG) = \frac{143.97}{\rho(cm)q} \sqrt{M(amu)\cdot E(MeV)}$$

with q in terms of unit charge. This expression, valid for non-relativistic systems, is applicable to detection of

evaporation residues.

The q value in the formula represents the charge state of the residue atom emerging from the target foil. For its determination, one may refer to Betz,[12] whose results appear in fig. 7, and note that for Z = 86 and an energy of about 30 MeV, the equilibrium charge state of the particle is seen to be about 17^+. For the design radius of 170 cm for the two independent fields, the requisite field is B = 3.90 kG. The E field is found from its relation to v_o and B,

$$E(v/m) = 3 \cdot 10^7 \sqrt{\frac{2 \cdot T(MeV)}{931.5 \cdot m(amu)}} \; B(kG)$$

which yields, for this case, $E = 2.07 \cdot 10^6$ v/m or a voltage difference between the plates of 52.7 kV.

The first priority was to adjust the velocity selector baffles to deny the beam tail entry into the system. A 150 MeV ^{37}Cl beam bombarded a natural Sn target, and the baffles were adjusted to optimize the fusion to elastic count ratio, while keeping the background level on the detector within tolerable limits. Counts were measured with a solid state detector positioned at the exit of the filter and were housed in an auxiliary chamber. Field settings were V_{vs} = 57.95 kV and B_{vs} = 3.42 kG, calculated in a manner identical to the procedure above. Natural tin was used

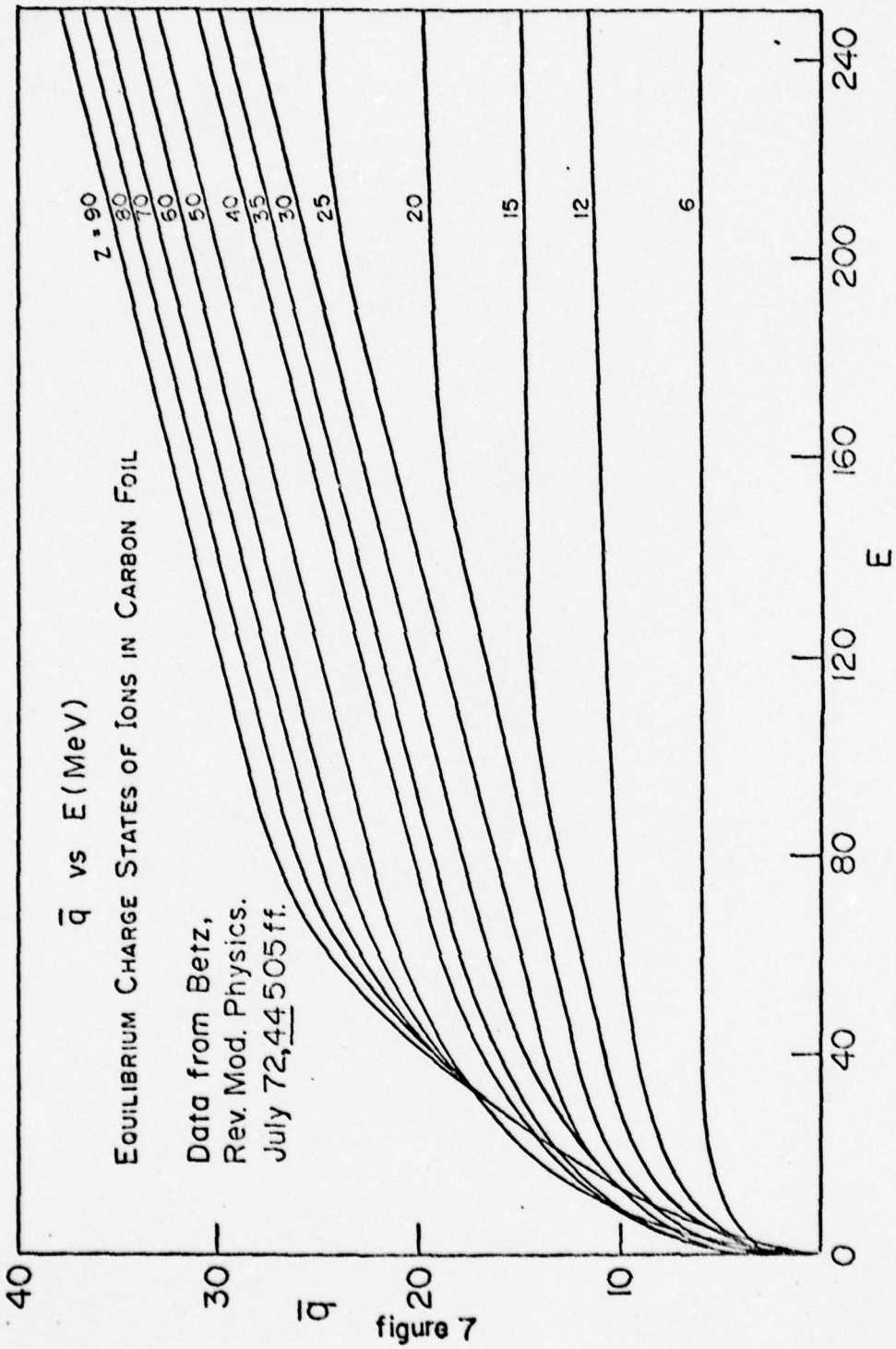
$\bar{q}$ vs E(MeV)
Equilibrium Charge States of Ions in Carbon Foil
Data from Betz,
Rev. Mod. Physics.
July 72,44 505 ff.
Z = 90
80
70
60
50
40
35
30
25
20
15
12
6
$\bar{q}$
E
0
40
80
120
160
200
240
10
20
30
40

figure 7

instead of thulium because its high yield reduced the exposure time required for good statistics.

With the baffles set, the range of velocities of the evaporation residues produced from thulium were examined. The beam energy was 175 MeV. The target was a double film of approximately 350 microgram/cm^2, backed by formvar, and made by vaporizing thulium out of a tantalum boat. The velocity profile was taken from -20% to +12% of v_o by varying the electric field of the velocity selector.

Due to loading limitations, a field of 3.90 kG could not be stabilized, so instead one of 3.85 kG was used, and a correspondingly diminished voltage difference of 51.5 kV was applied across the plates. The reduced fields result in a particle trajectory below the centerline of the velocity selector. This has been taken into account in determining the velocity dependence of solid angle. The result of this measurement appears in fig. 8. The broken line represents an estimated background level, consisting mostly of knockouts.

Figure 9 shows the result of an angular distribution of the evaporation residues, taken from 0° to 8°, under the same conditions as the velocity profile. The background estimation of fig. 8 has been subtracted.

With the target removed, the beam was run until over 200,000 elastics were collected by the monitors. No counts were detected in the detector at 2.5°, confirming that the

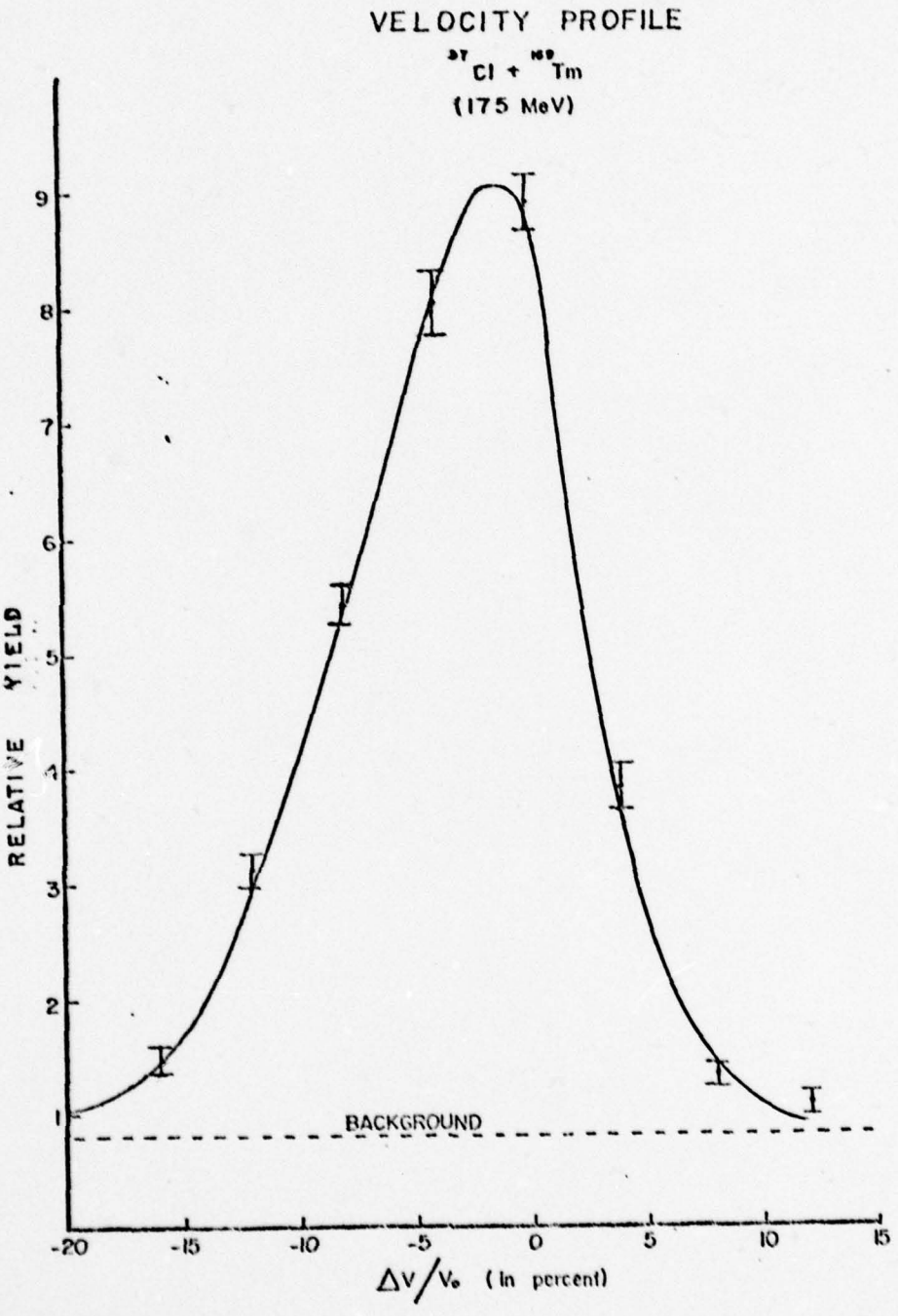
VELOCITY PROFILE
37Cl + 169Tm
(175 MeV)
RELATIVE YIELD
9
8
7
6
5
4
3
2
1
BACKGROUND
-20
-15
-10
-5
0
5
10
15
ΔV/Vo (in percent)

figure 8

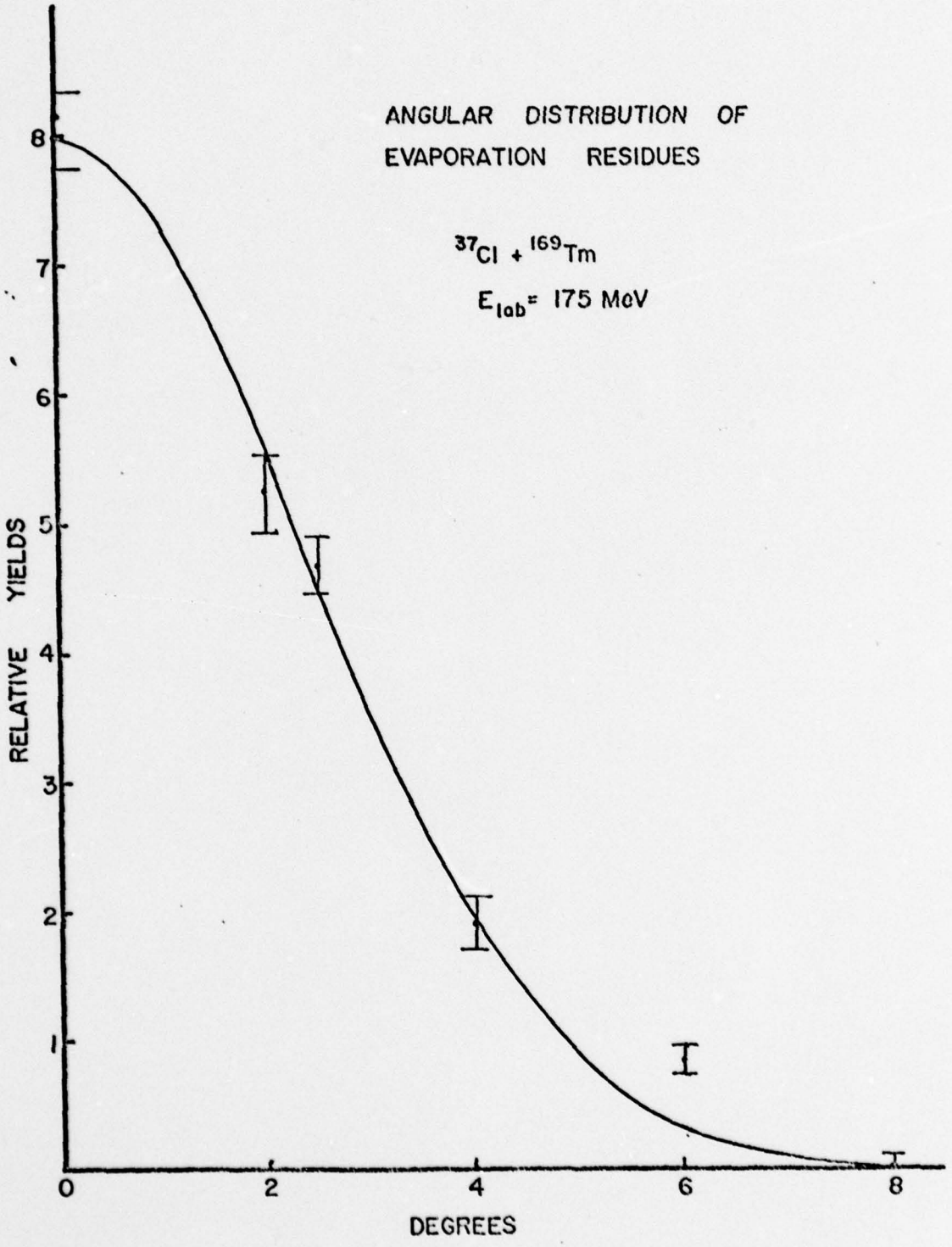
ANGULAR DISTRIBUTION OF
EVAPORATION RESIDUES
$^{37}Cl + ^{169}Tm$
E_{lab}= 175 MeV
RELATIVE YIELDS
0
1
2
3
4
5
6
7
8
0
2
4
6
8
DEGREES

FIGURE 9

low energy beam tail had been eliminated by the trap.

The magnetic quadrupoles and dipole were than optically aligned by sighting through the beam pipe with a Taylor-Hobson telescope mounted on the upstream reference sight mount.

To fine tune the system, a 450 mm^2 solid state detector was mounted at the calculated focal point in the velocity port at 0°. Using a 150 MeV ^{37}Cl beam on a tin target, the appropriate field settings for the velocity selector were set, currents corresponding to the B fields as calculated by Raytrace were sent through the quadrupoles. The ratio of fusion counts to elastics was taken as a function of the quad potentiometer reading. That plot is shown in fig. 10. From this it is clear that prime focusing occurs with a ratio of quad setting to B_{vs} of .3924. A consideration of the geometry involved will convince one that in order to preserve a radius of curvature for any particle velocity, focusing on the detector will result when that ratio of .3924 is maintained.

As a check of the alignment of the system and the focusing of the quads, three strips of Lexan were mounted in place of the solid state detector, and the quad settings varied. As seen in fig. 11, the peak of the residues was displaced by 7 mm laterally from the beam pipe centerline.

With the detector reinstalled, the residues were swept vertically by an application of small currents through the

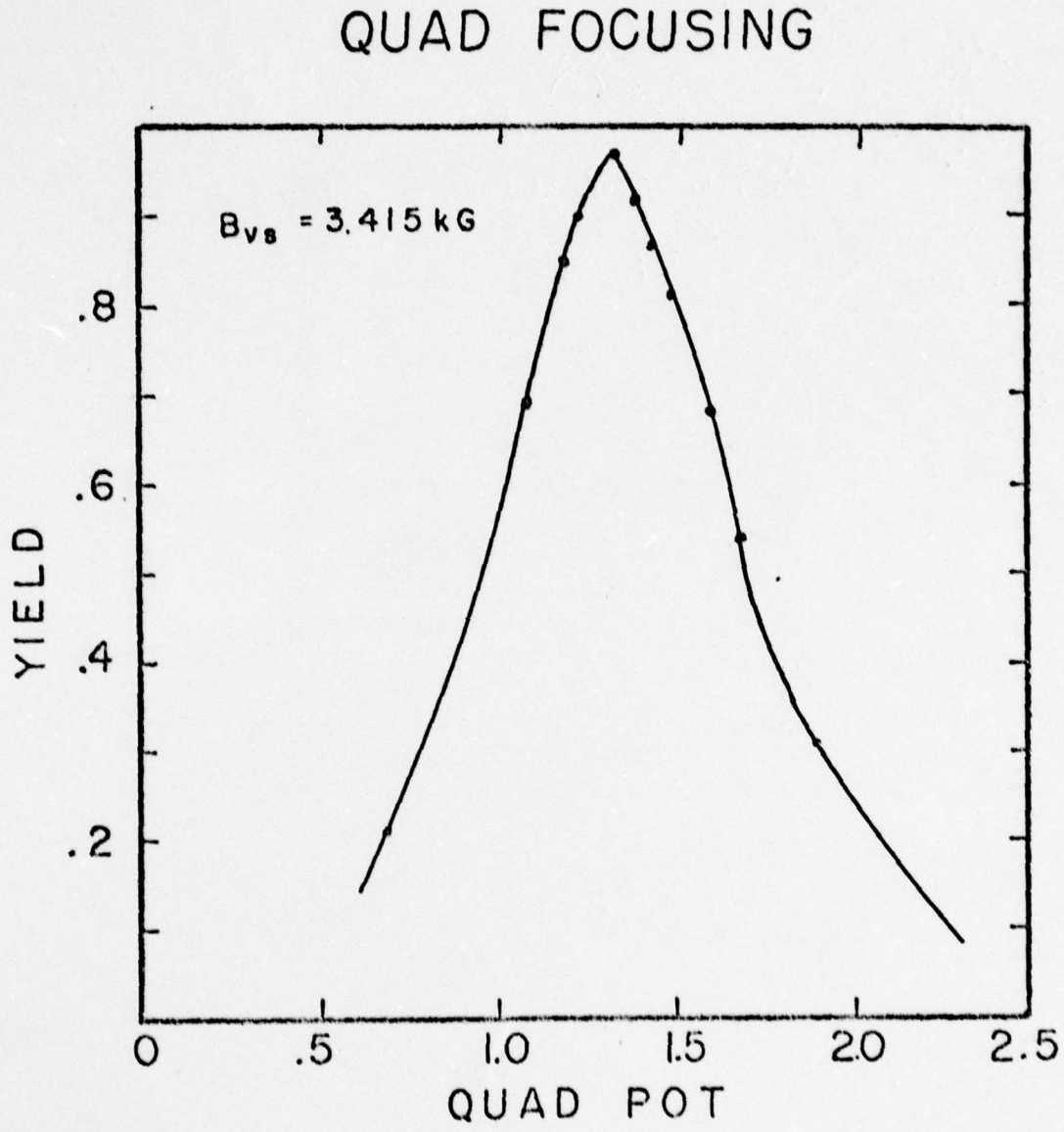

figure 10

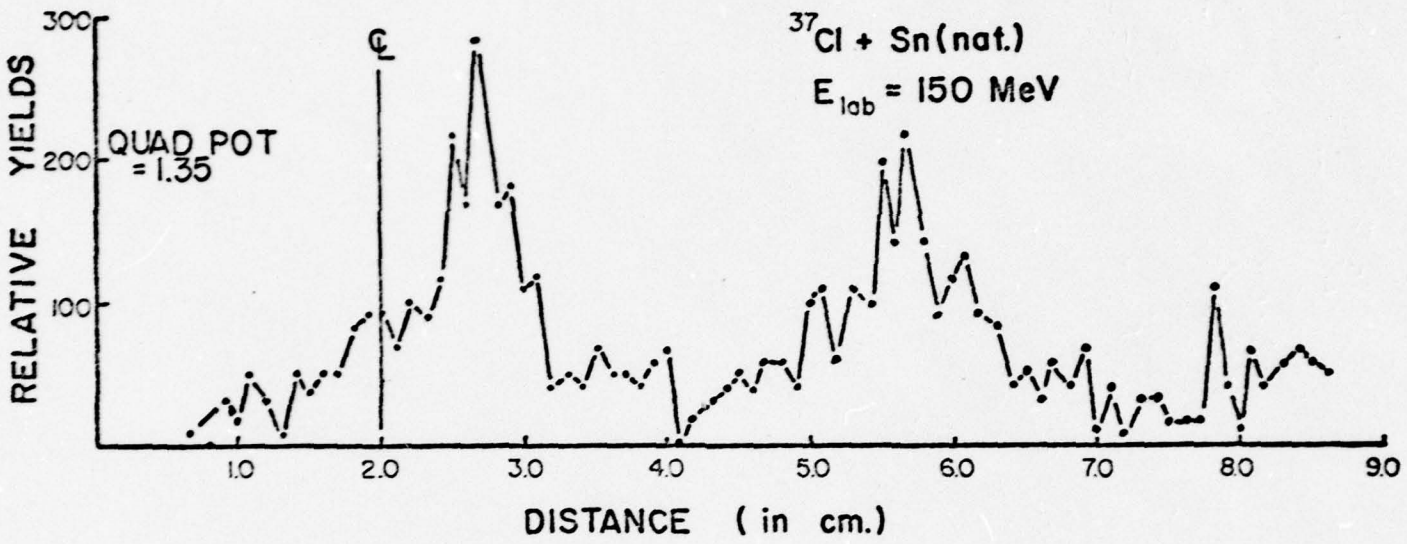

FIGURE 11

EVAPORATION RESIDUE IN LEXAN

dipole. The detector itself was moved horizontally by means of the sliding arm on which it was mounted. The greatest number of counts resulted with a 2 ampere current through the dipole, and with the detector 7 mm to the right of the geometric center of the chamber, confirming the results of the Lexan run. With the system tuned, work was begun on thulium.

Figure 12 depicts the electronics set up in this experiment. The 25 mm^2 solid state monitors and related circuitry served in normalizing counts to a constant time integrated current. The 600 mm^2 solid state detector was connected to a BNL fast timing preamplifier with a very short cable to keep circuit capacitance to a minimum. A timing single channel analyzer set with its lower level just above the inherent noise level, and its upper level open, provided the "all gate," for particles of all energies striking the detector. A 550 microgram/cm^2 thulium target was used.

A second TSCA was set to discriminate against all but energies in the calculated range of the evaporation residues. When this TSCA measured a particle of the proper energy, a number of processes were initiated. A fusion gate pulse was sent to the computer; a multiscalar was started which in turn reset and started a "clock" in the computer, as well as diverting the beam from the target by energizing an electro-

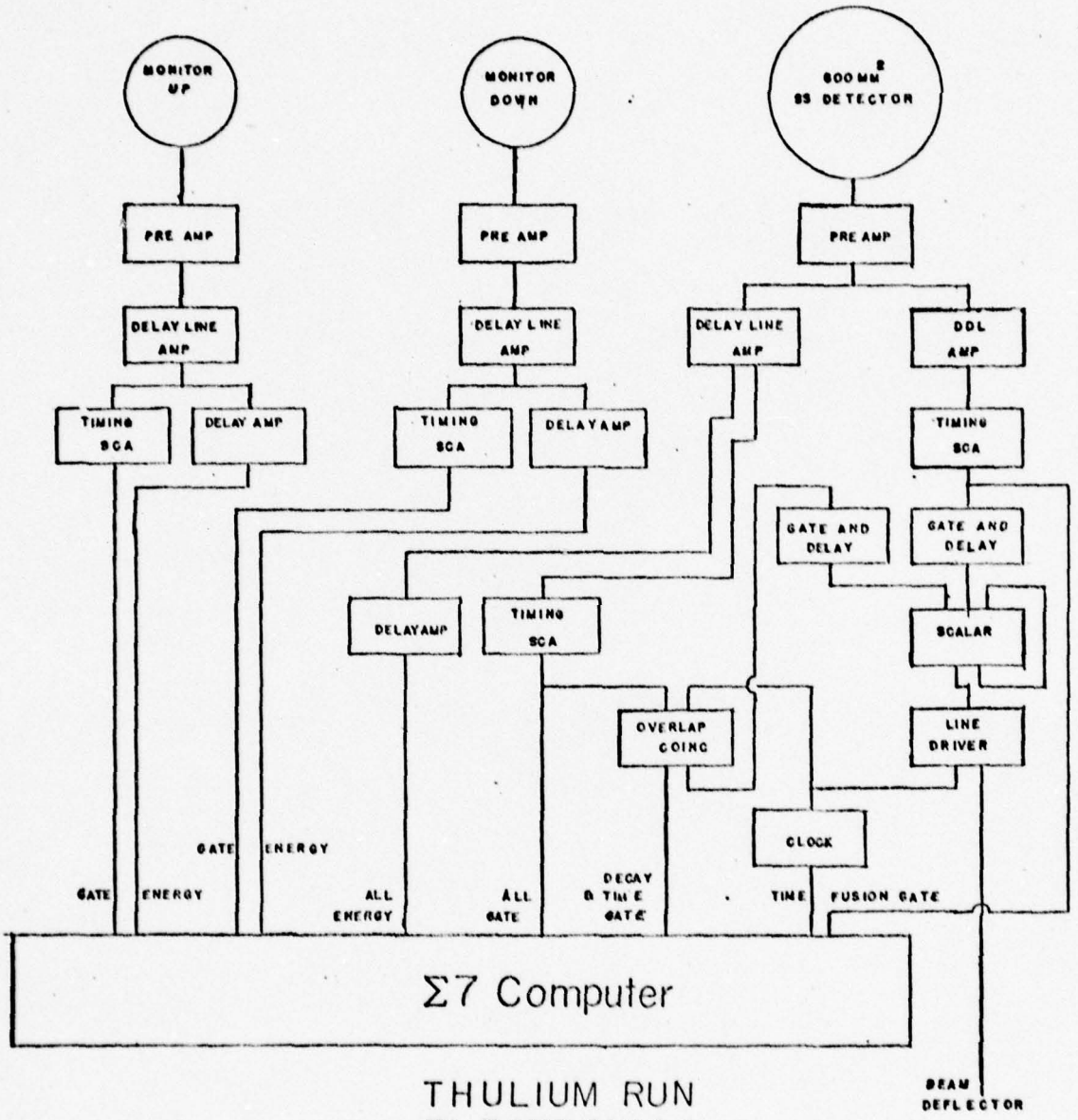

THULIUM RUN
ELECTRONICS

figure 12

static deflector. The multiscalar when running put a +5 volt bias on an overlap/coincidence unit. With the beam diverted, the system awaited another event, presumably an alpha decay from an evaporation residue, but also perhaps the products of its fissioning. A particle of any energy would cause the "all" TSCA to send a +5 volt level to the other side of the coincidence unit, from which would issue a decay and time gate to the computer, the "and" requirement being met. Another logic pulse would be sent to the multiscalar to stop it, which would result in the beam being redirected, and the "fusion" bias on the coincidence unit would vanish. Additionally, the multiscalar would self stop after an elapsed time of 20 sec, the equivalent of about two expected lifetimes.

Recorded were the energy spectra of all particles, fusion products, out-of-beam decays, and both monitors. A time, and a two dimensional time vs out-of-beam energy spectrum was also taped. Representative spectra appear in figs. 13 through 18. The entire run was conducted at 178 MeV.

Two modifications to the electronics were made prior to subsequent runs, as shown in fig. 19. These comprised the integration of a mechanical chopper, in conjunction with the electrostatic deflector, to eliminate the beam; and the addition of a mechanical timer to deny entry into the circuit

'ALL' ENERGY

$^{37}Cl + ^{169}Tm$ 178 MeV

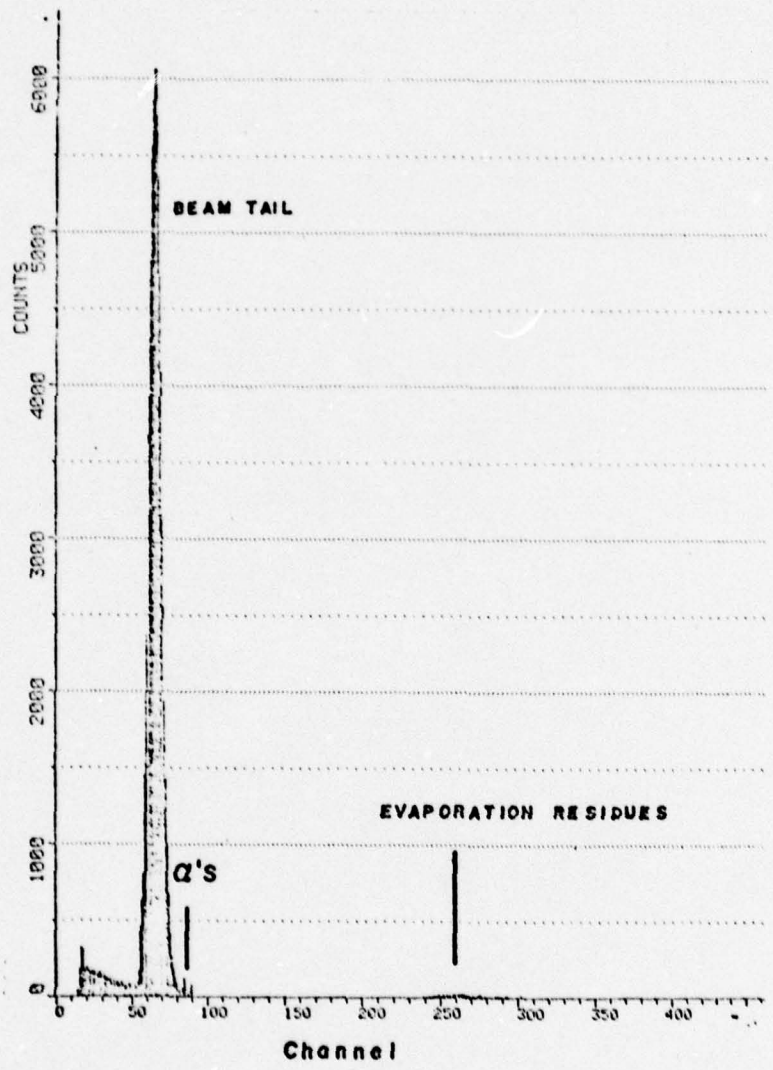

figure 13

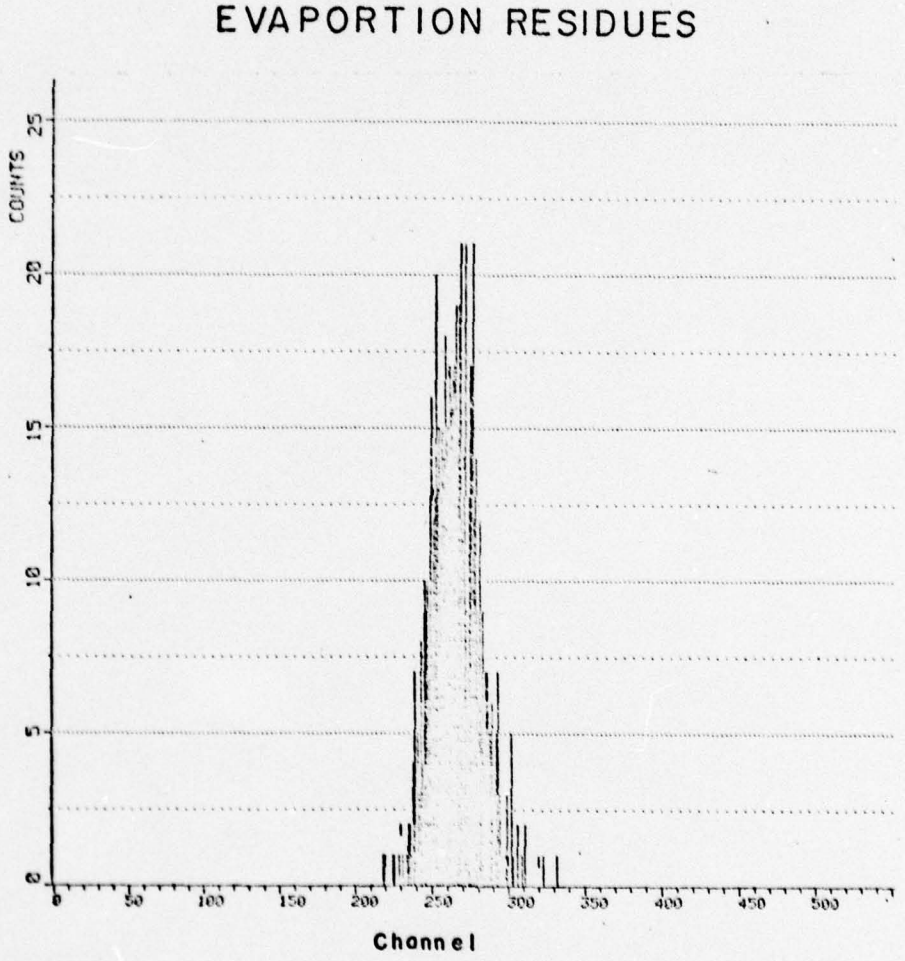
EVAPORTION RESIDUES
COUNTS
0
5
10
15
20
25
0
50
100
150
200
250
300
350
400
450
500
Channel

figure 14

OUT OF BEAM SPECTRUM

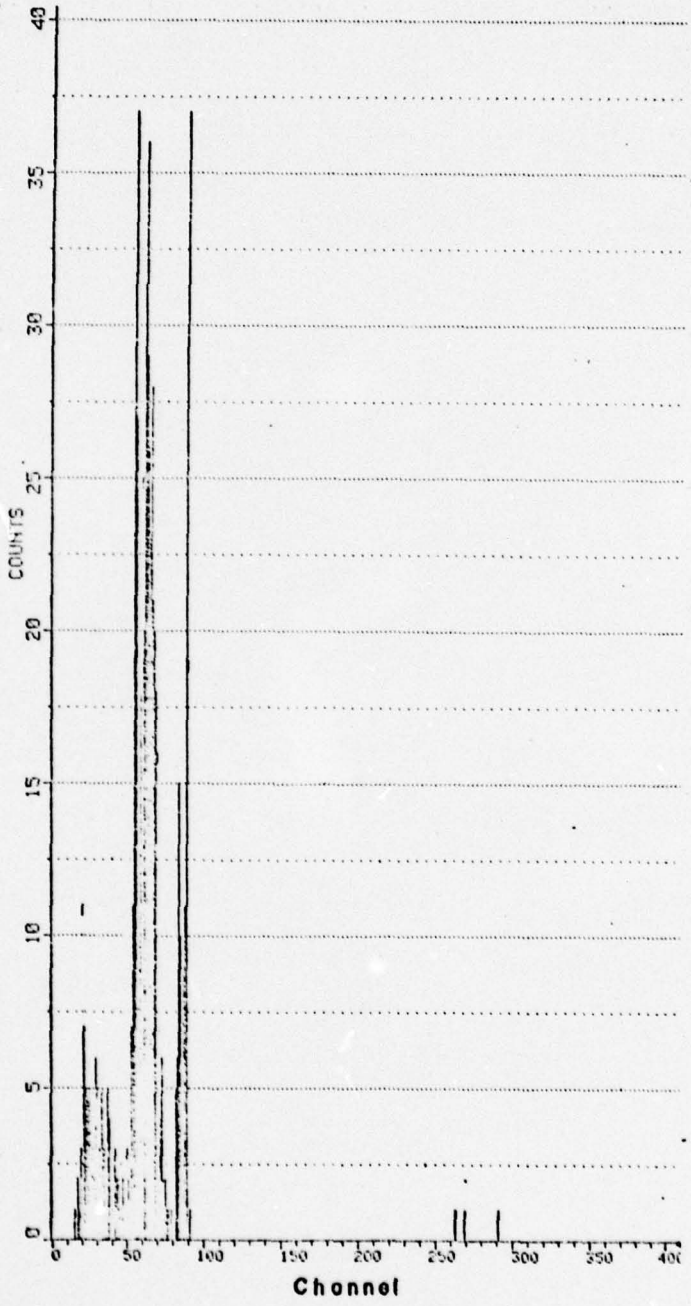

figure 15

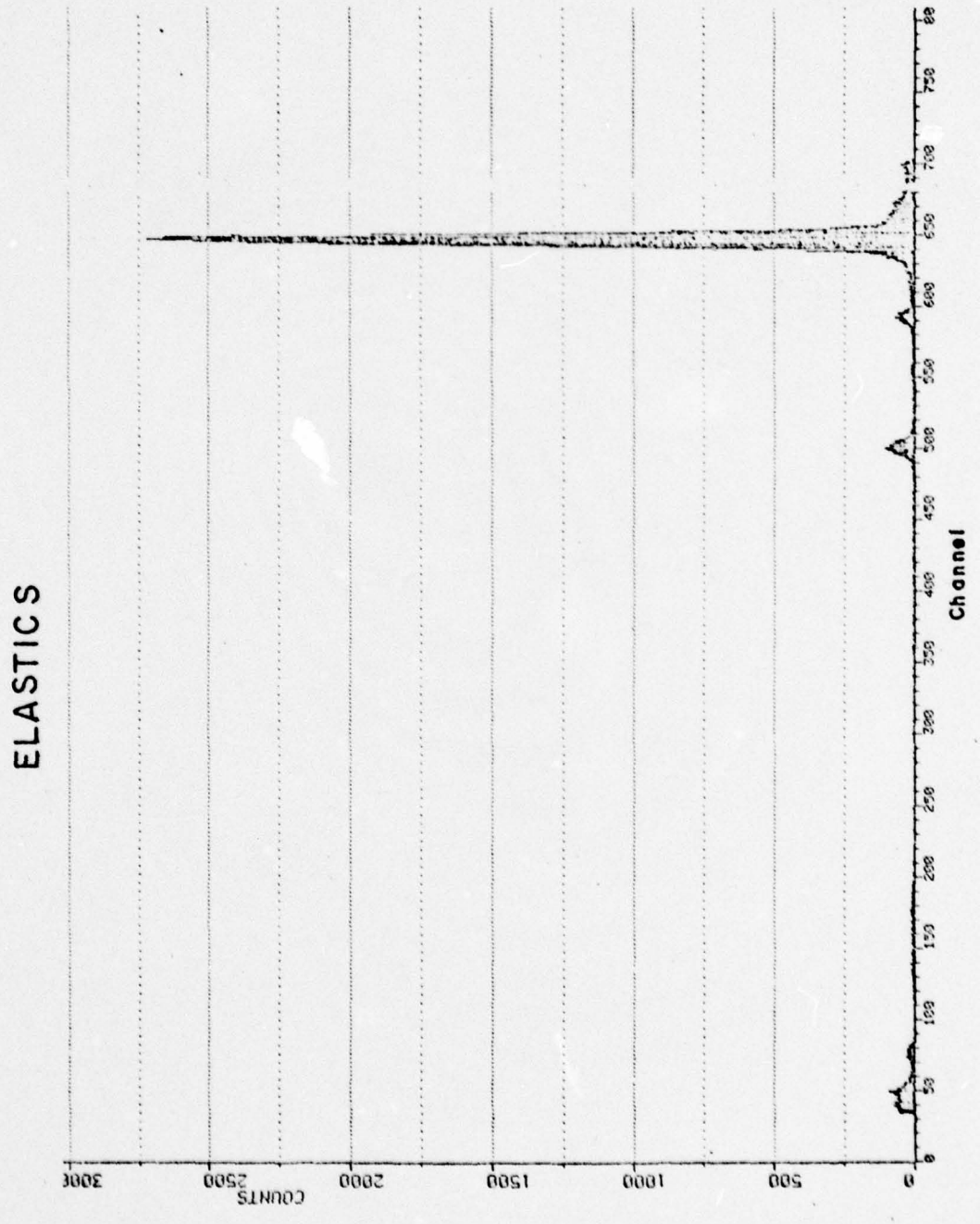

figure 16

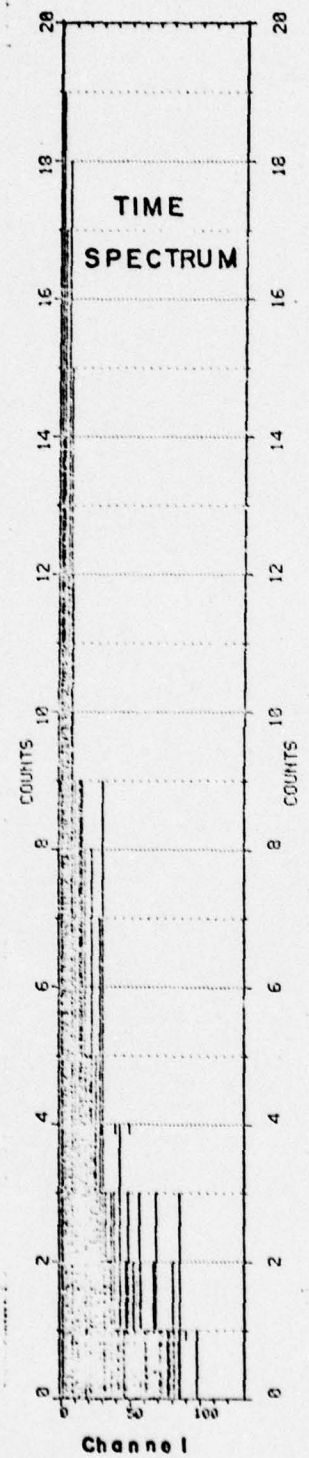

figure 17

ENERGY VS TIME

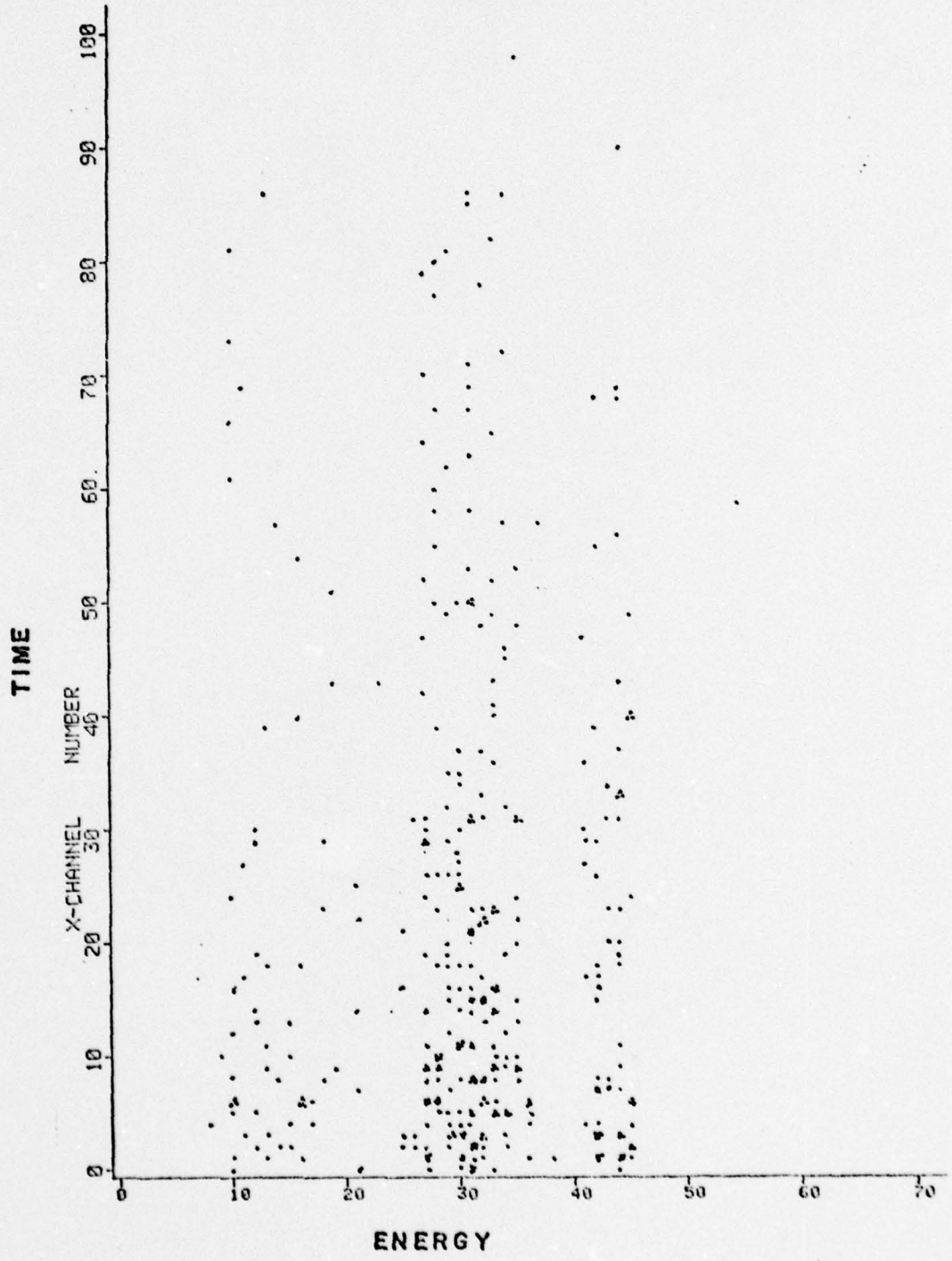

figure 18

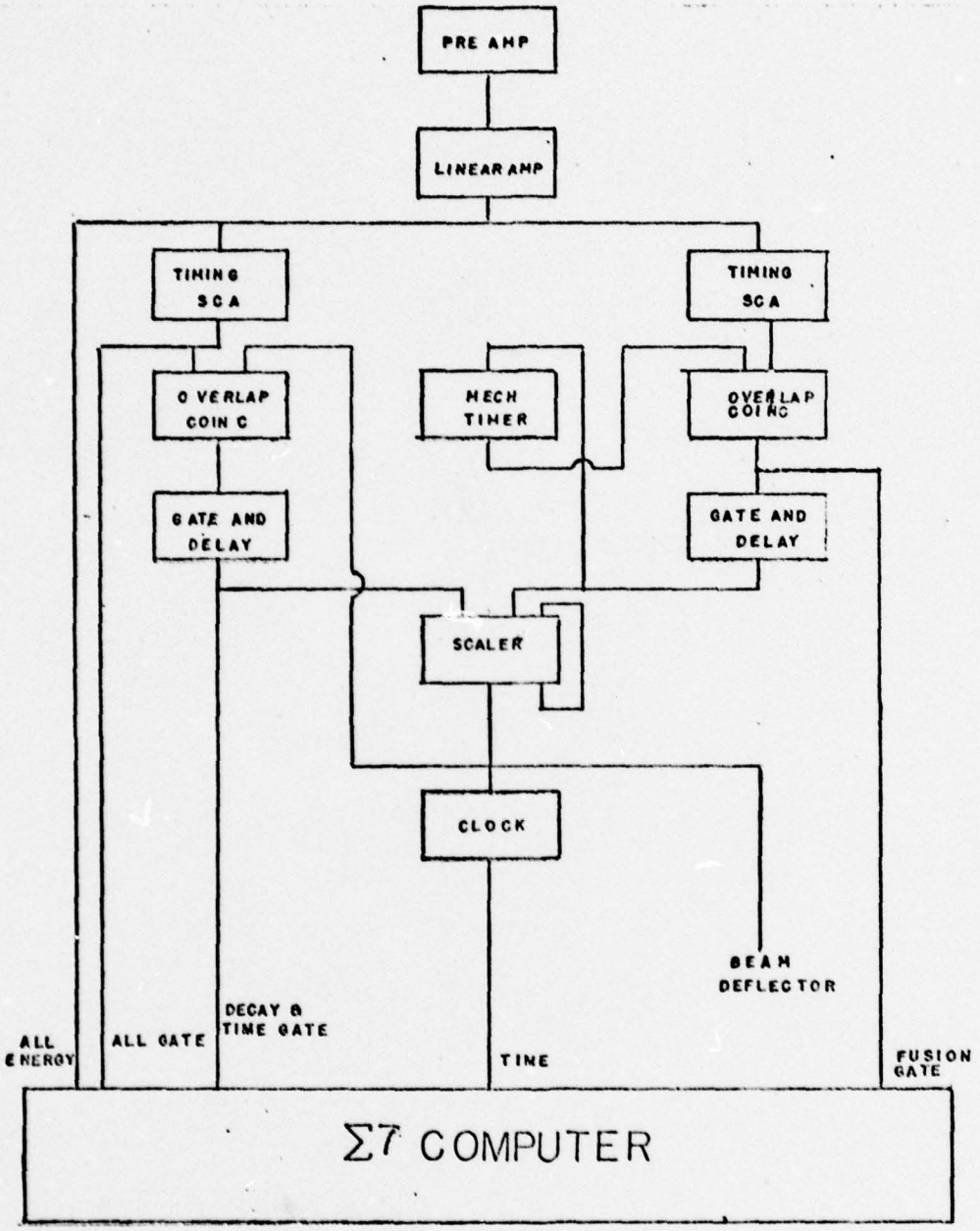

IMPROVED
ELECTRONICS

figure 19

of a subsequent fusion event after the deflector had been triggered but before it had become effective.

A check was then made of the centering of the residues on the detector at 179 MeV with a ^{169}Tm target by altering the dipole field. The count rate peaked with a field of 0.06 kG on the dipole, with the detector offset horizontally 8 mm. The other fields were set at V_{vs} = 52.3 kV, B_{vs} = 3.88 kG, and quad potentiometer = 1.52.

An energy calibration was obtained using a ^{241}Am open source, emitting alphas of 5.4857 MeV. A linearity check was made of energy channels using a pulser.

With the mechanical chopper removed, and the beam at 176 MeV, spectra from the monitors, from the gated and ungated detector, time, and energy vs time spectra were taken. The separation of the alphas from the beam tail is clear from fig. 20.

The horizontal offset of the focusing was corrected by rotating the quadrupoles about a vertical axis by 0.25°. The result of this adjustment was verified using a 25 mm^2 detector in the velocity port. To remedy the vertical offset, the dipole was lowered the appropriate amount.

A fresh target 350 microgram/cm^2 thick with formvar backing was then mounted. The 600 mm^2 detector was replaced by one of 450 mm^2 of significantly better energy resolution, and biased at 150 v. The electronics of this run appears in

'ALL' ENERGY

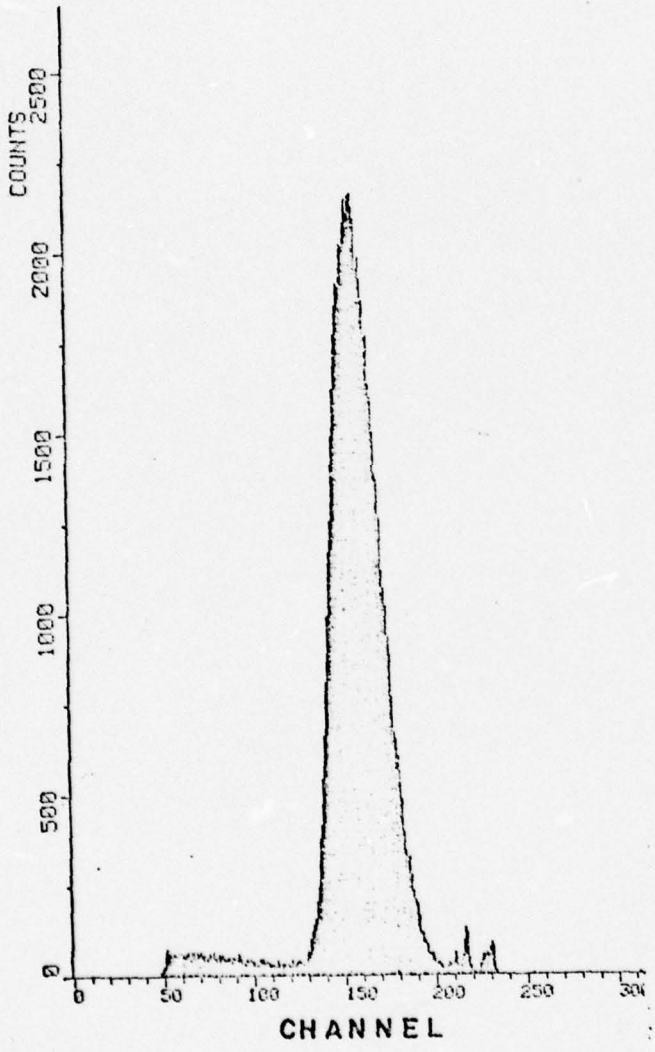

figure 20

fig. 21. The inhibitor against subsequent fusion products was removed, and a binary scalar timed by an HP3320B synthesizer with a dual discriminator served as the clock, since the formerly used Ortec 417 timer was unavailable. With two-stage operation of the tandem and using the enriched cone source, excitation functions were measured at 151 to 186 MeV in increments of 5 MeV in the velocity port. A direct current mode was employed, since the anticipated 6.5 MeV alphas would be quite distinct from the 4.5 MeV beam particles passing through the velocity selector, as seen in earlier runs. At each energy, counts on the detector and monitors were recorded. A typical spectrum showing the alphas well separated from the beam is seen in fig. 22.

An internally mounted ^{241}Am source provided calibration data. Peak readings of these 5.4857 MeV alphas were measured with the detector parallel and at $\pm 60°$ with the source, so as to allow determination of the detector's insensitive layer. With the source at 60° and the detector at 90°, the dead layer of the source could be determined.

A timing run at 166 MeV, where the excitation function comprised essentially only two species, was conducted with a 0.4 sec per channel allocation. The timer ran for 40 sec while the circuit awaited an out-of-beam decay; the clock would not stop in the event of such a decay, but would run

FINAL ELECTRONICS

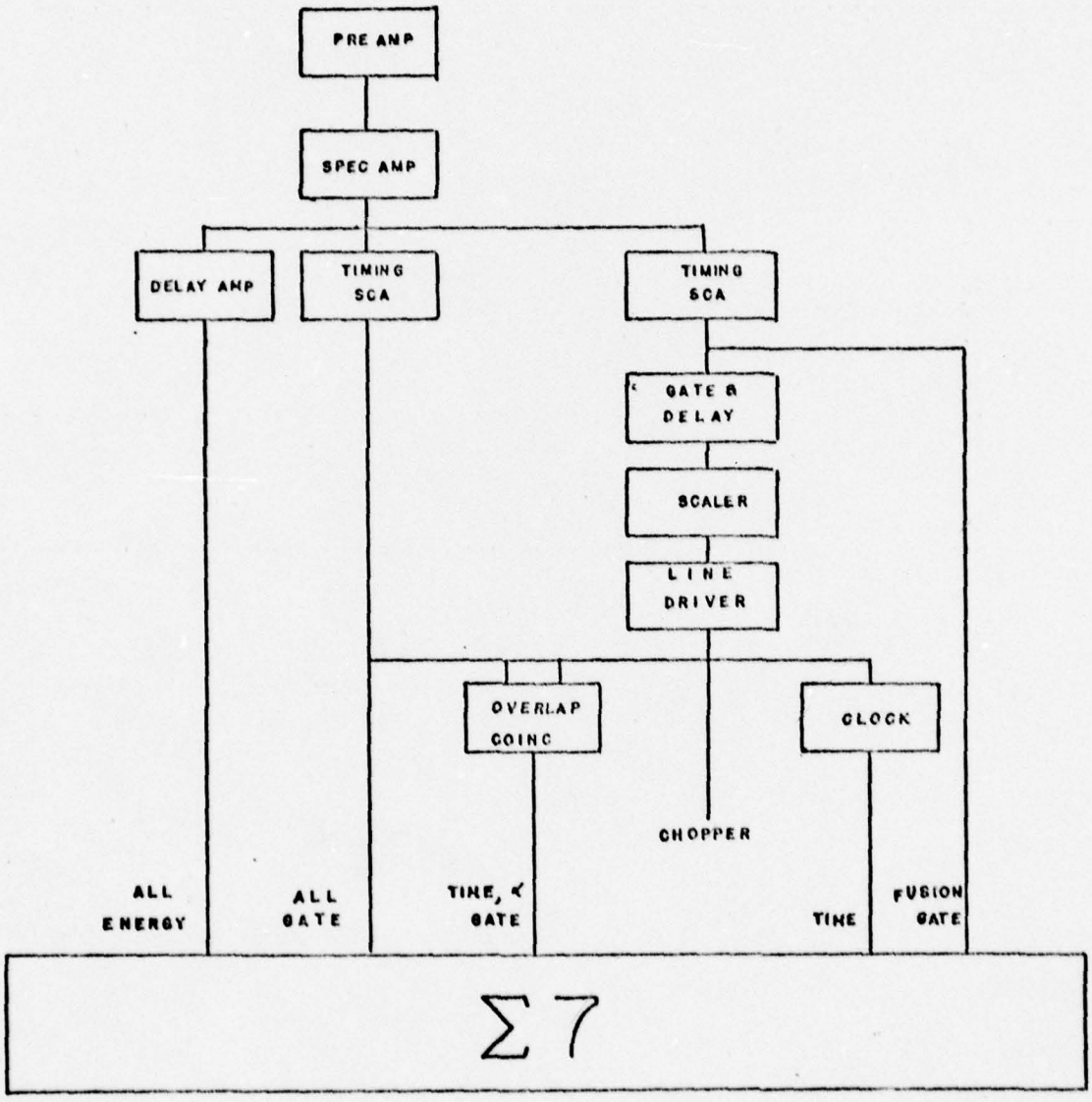

figure 21

'ALL' ENERGY

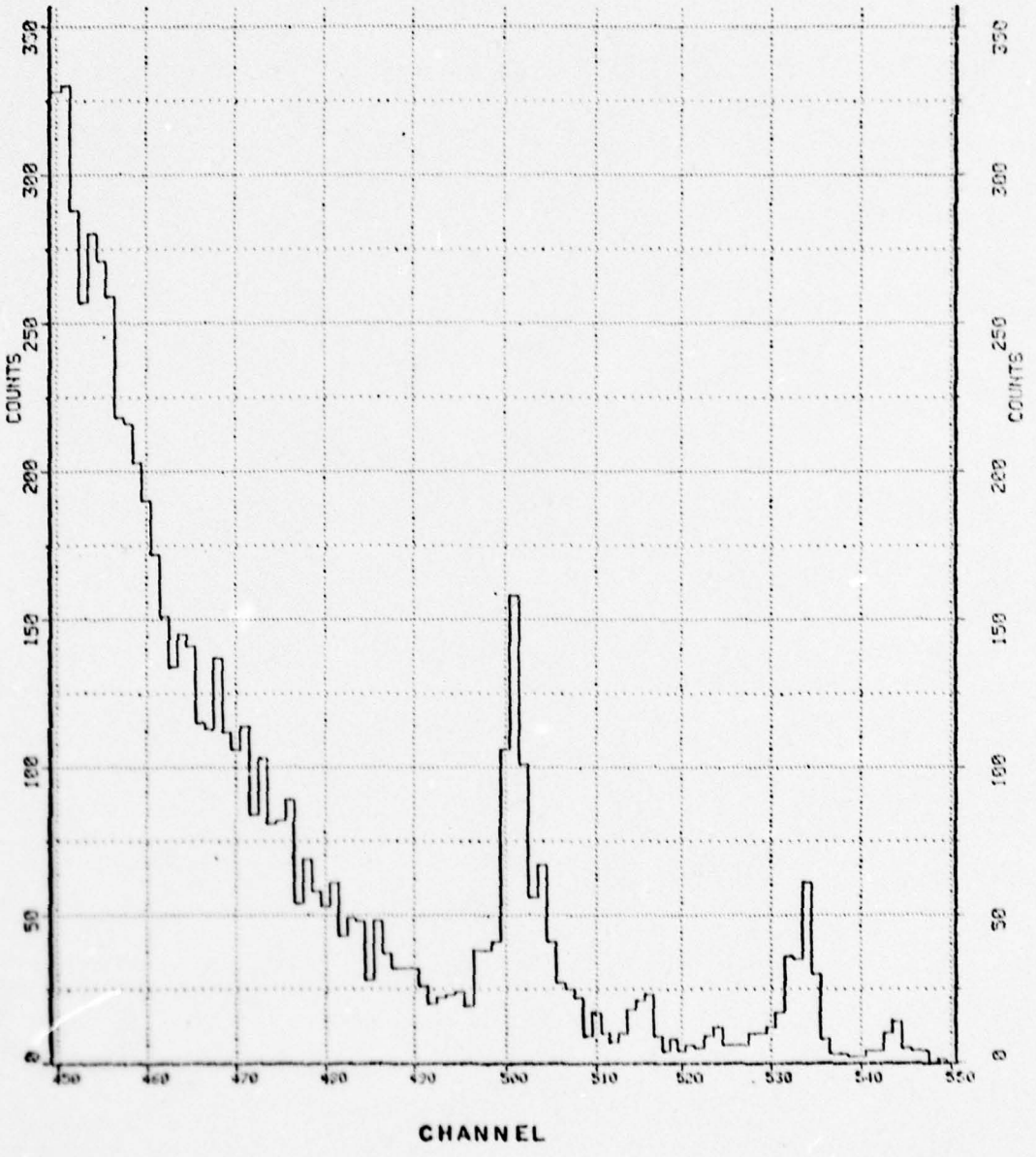

figure 22

the full 40 sec. In addition to the event lines already noted, a 2D energy-time spectrum, and a special time spectrum for alphas of energy equal to those from ^{202}Rn were recorded. The special time spectrum appears in fig. 23. Although this is not the optimal way to obtain lifetime information with a high fusion count and long alpha lifetimes, it may be ideal for more massive systems of low cross section and short half lives.

B. Results and Analysis

Any cross section determination from the data collected in this experiment requires that a normalization of collected counts be made to account for fluctuations in beam intensity and duration of exposure. To this purpose are mounted the two monitor detectors in the target chamber. Mounted in the vertical plane of the beam line, they subtend solid angles of .159 and .158 millisteradians, upper and lower, respectively. Employment of a pair reduces the sensitivity of the total counts to shifts in beam position or orientation. For angles of about 30°, all elastics collected by the monitors are Rutherford scattered for the lab energies employed here. Thus, independent of beam charge state and target thickness, normalization is straightforward, since for a constant number of collected elastics there corresponds a reasonably constant exposure, keeping in mind the E^{-2}

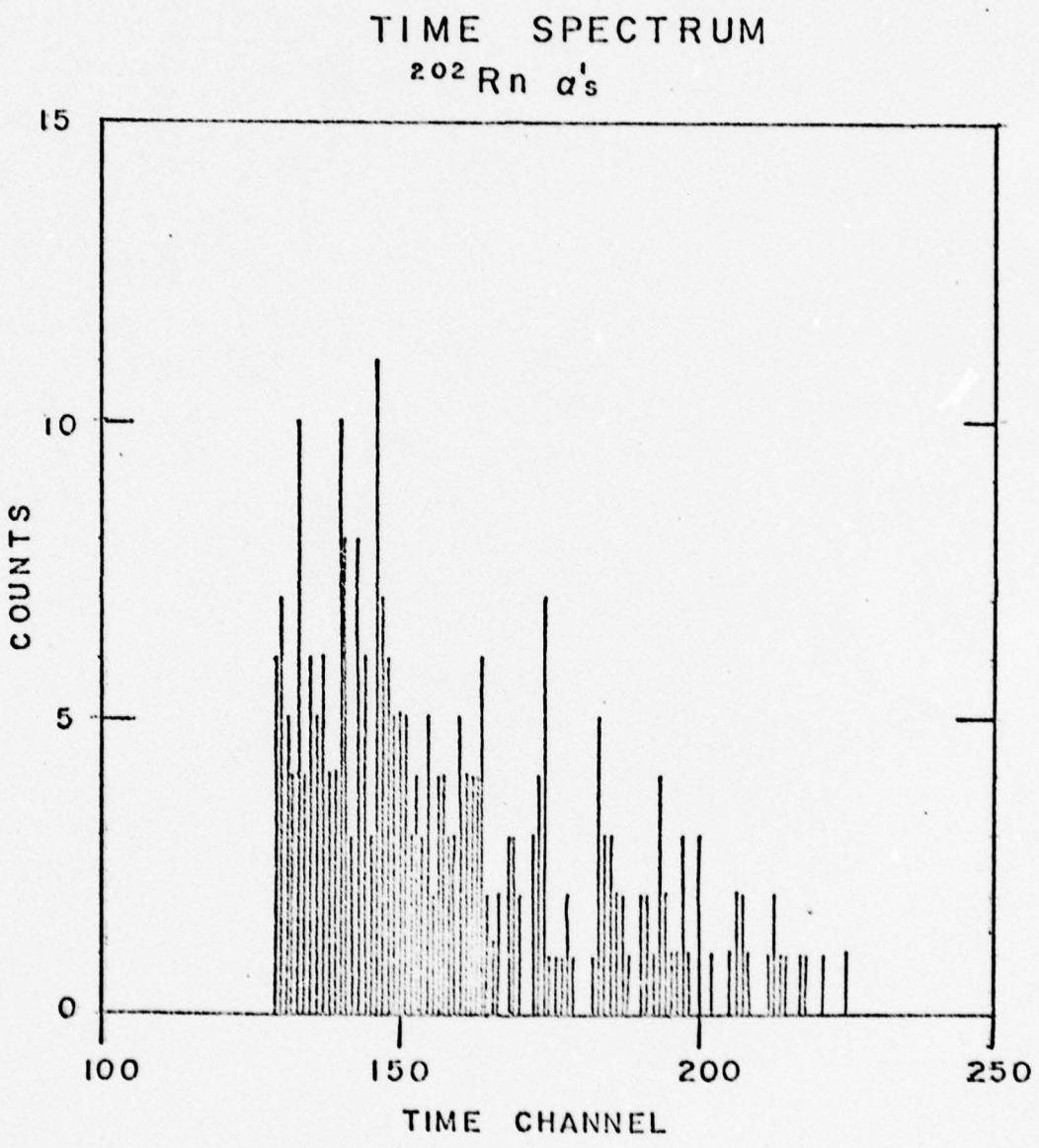
TIME SPECTRUM
^{202}Rn α's
15
10
5
0
COUNTS
100
150
200
250
TIME CHANNEL

figure 23

dependence of this type scattering cross section.

In fig. 22 , one easily distinguishes the alpha peaks separated from the low energy ^{37}Cl beam tail, the velocity of which having allowed it to pass through the velocity selector. The beam tail's energy, simply that of the evaporation residues multiplied by a factor equal to the ratio of the mass of chlorine to that of the residue, is roughly 5.5 MeV, while that of the alphas is known to be about 6.5 MeV.

The relevant portion of the chart of nuclides appears in fig. 24, showing the decay schemes of the expected evaporation residues and their daughters. The energies listed are those of the emitted alpha particles.

The velocity profile of fig. 8 reveals a σ = 4.9% and a background, consisting mainly of thulium knockouts resulting from the back scattering of low energy chlorine. The background, estimated at 0.8, has been subtracted from the angular distribution of fig. 9, and a gaussian fitted to the data,[13] yielding a σ = 2.37°. Ideally a velocity profile should have been measured at representative points in the angular distribution, but constraints on beam time precluded such a lengthy procedure.

The 178 MeV ^{37}Cl + ^{169}Tm run described yielded little useful information, except the fact that the positioning of the dipole needed correction, and that the electronic circuit

α DECAY SCHEMES

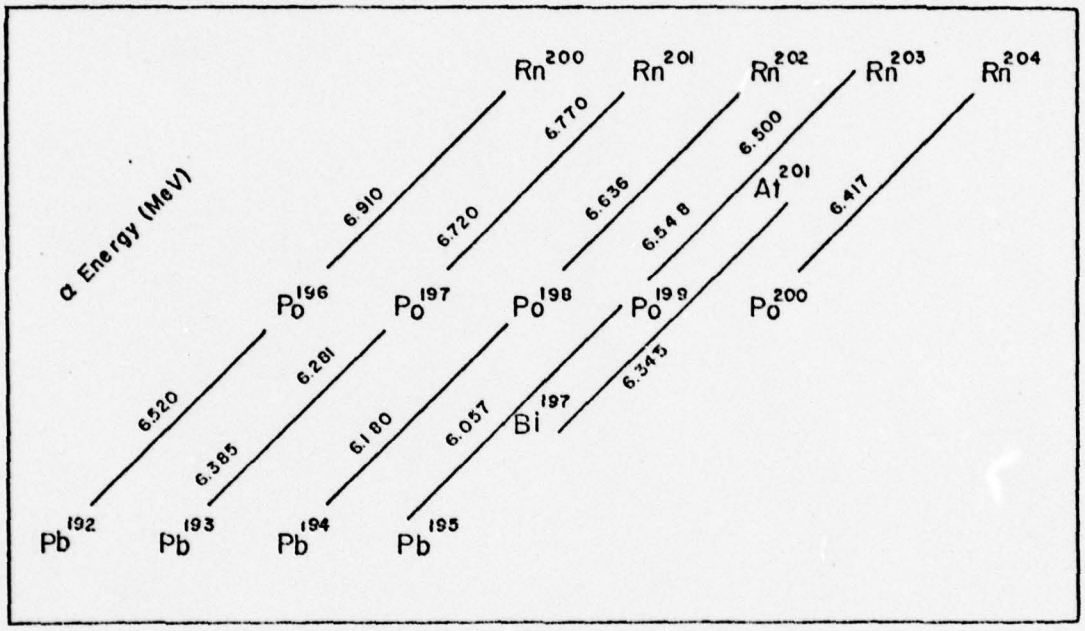

figure 24

was successful in diverting the beam after detecting an evaporation residue. However, the measured half life of 18.8 sec was much greater than the accepted value for any of the residues from the compound nucleus.

Modifications made prior to the 176 MeV thulium run were of marked value. Detected alphas had energies of 6.28, 6.44, 6.73, and 6.86 MeV, which are easily associable to those listed in fig. 24. Yet the half life measurements were much too short, indicating that the scalar should not have been stopped upon arrival of the first alpha.

The measured 0° excitation function data of parents are plotted and joined by smooth curves in fig. 25, as identified by the energies of emitted alphas. As the daughters of these also alpha decay, a similar plot for them appears in fig. 26.

In fig. 27 is shown the lifetime measurement of ^{202}Rn at 166 MeV. Data was ordered in groups of ten, and plotted. The solid line results from a computer weighted least squares fit program,[13] yielding a half life of 10.5±.9 sec. The accepted value is 9.9 sec.

Assignment of energies to the various channels is based on the ^{241}Am calibration and pulser test conducted before the timing run. The attenuation constant of the pulser plotted against the peak channel gives a straight line, with a channel of 13.4 corresponding to 0 volts. To the known alpha energy of 5.4857 MeV corresponds channel 432.

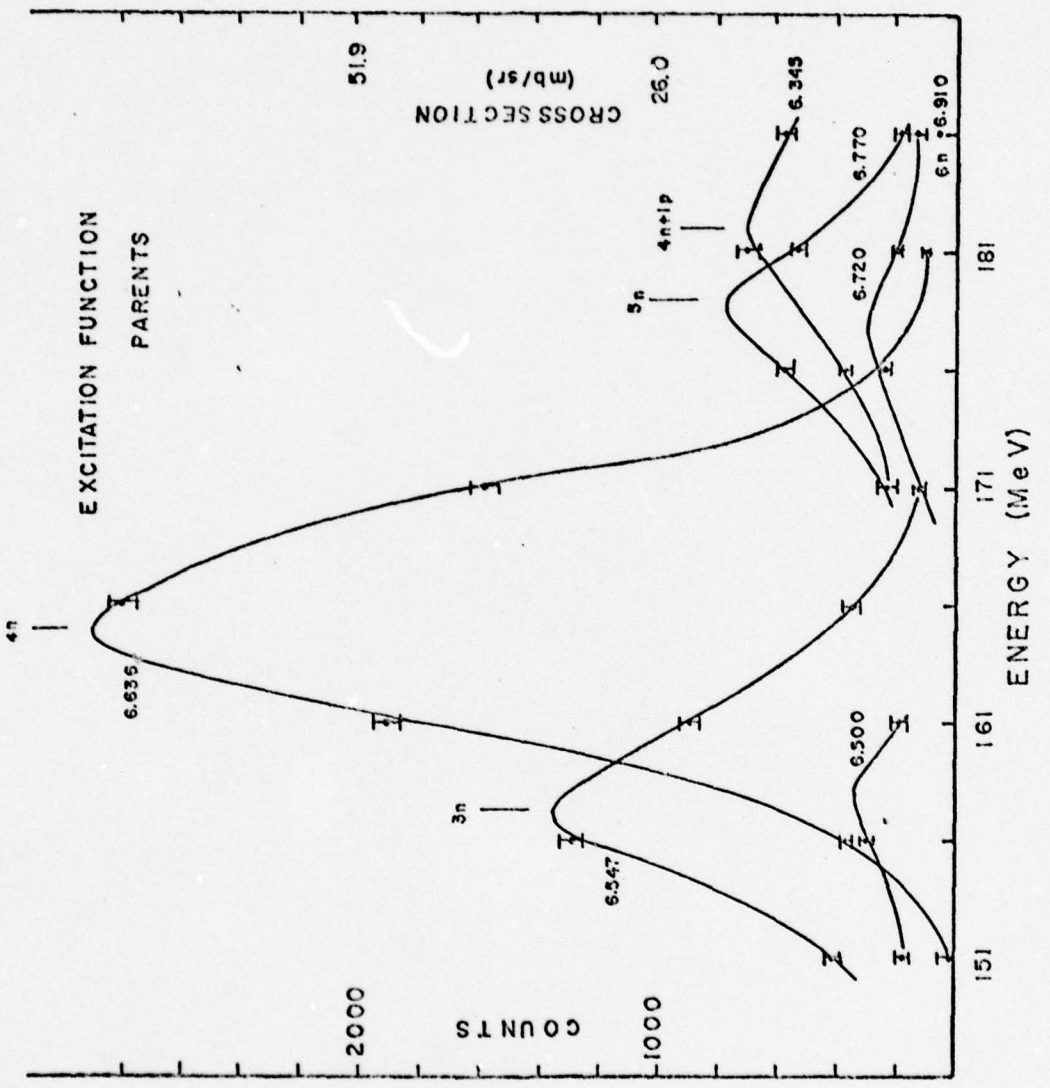
EXCITATION FUNCTION
PARENTS
CROSS SECTION
(mb/sr)
51.9
26.0
COUNTS
2000
1000
ENERGY (MeV)
151
161
171
181
4n
6.635
3n
6.547
5n
4n+1p
6.500
6.720
6.770
6.345
6n
6.910

figure 25

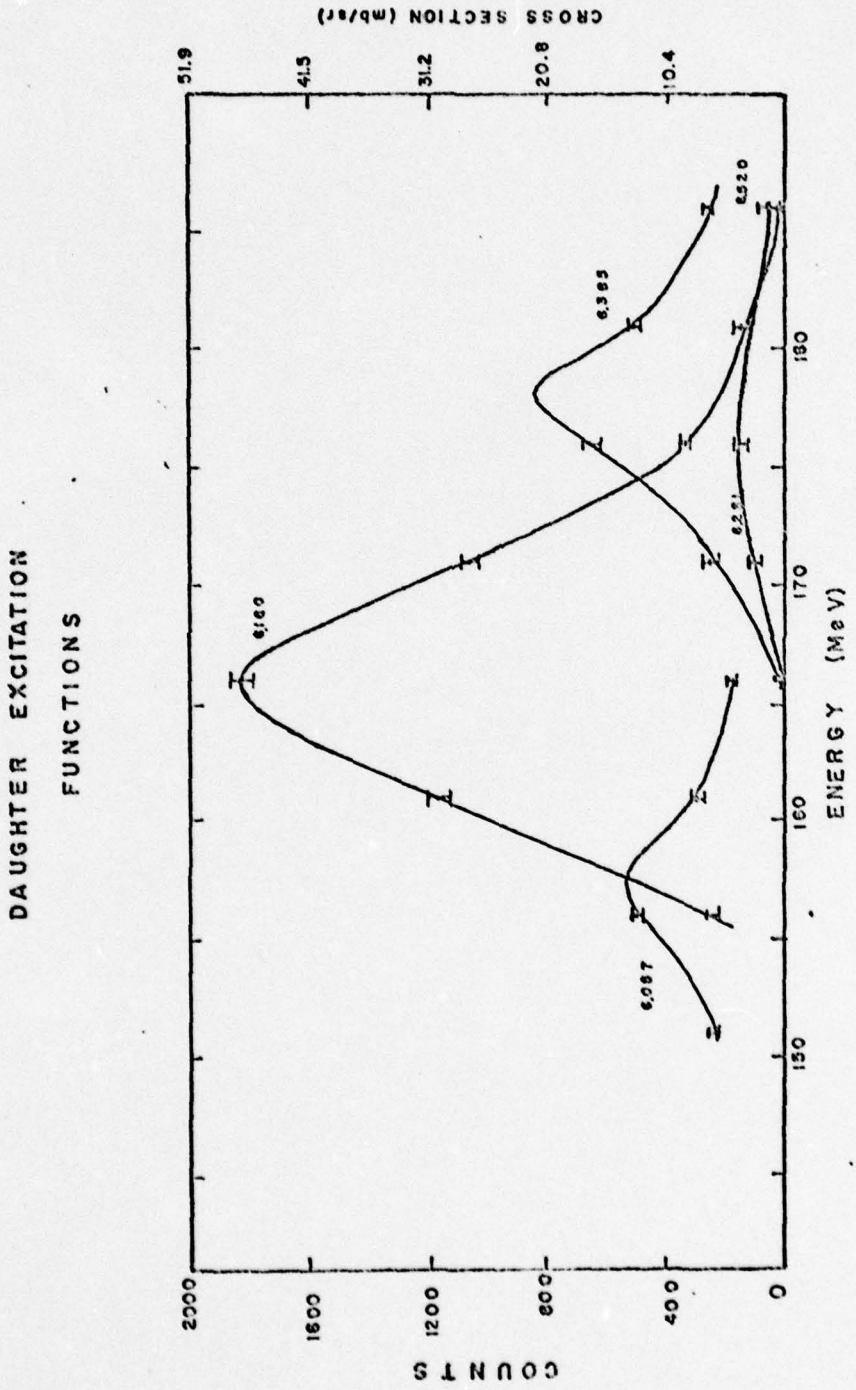
DAUGHTER EXCITATION FUNCTIONS
CROSS SECTION (mb/sr)
51.9
41.5
31.2
20.8
10.4
6.320
6.385
6.221
6.160
6.087
COUNTS
2000
1600
1200
800
400
0
150
160
170
180
ENERGY (MeV)

figure 26

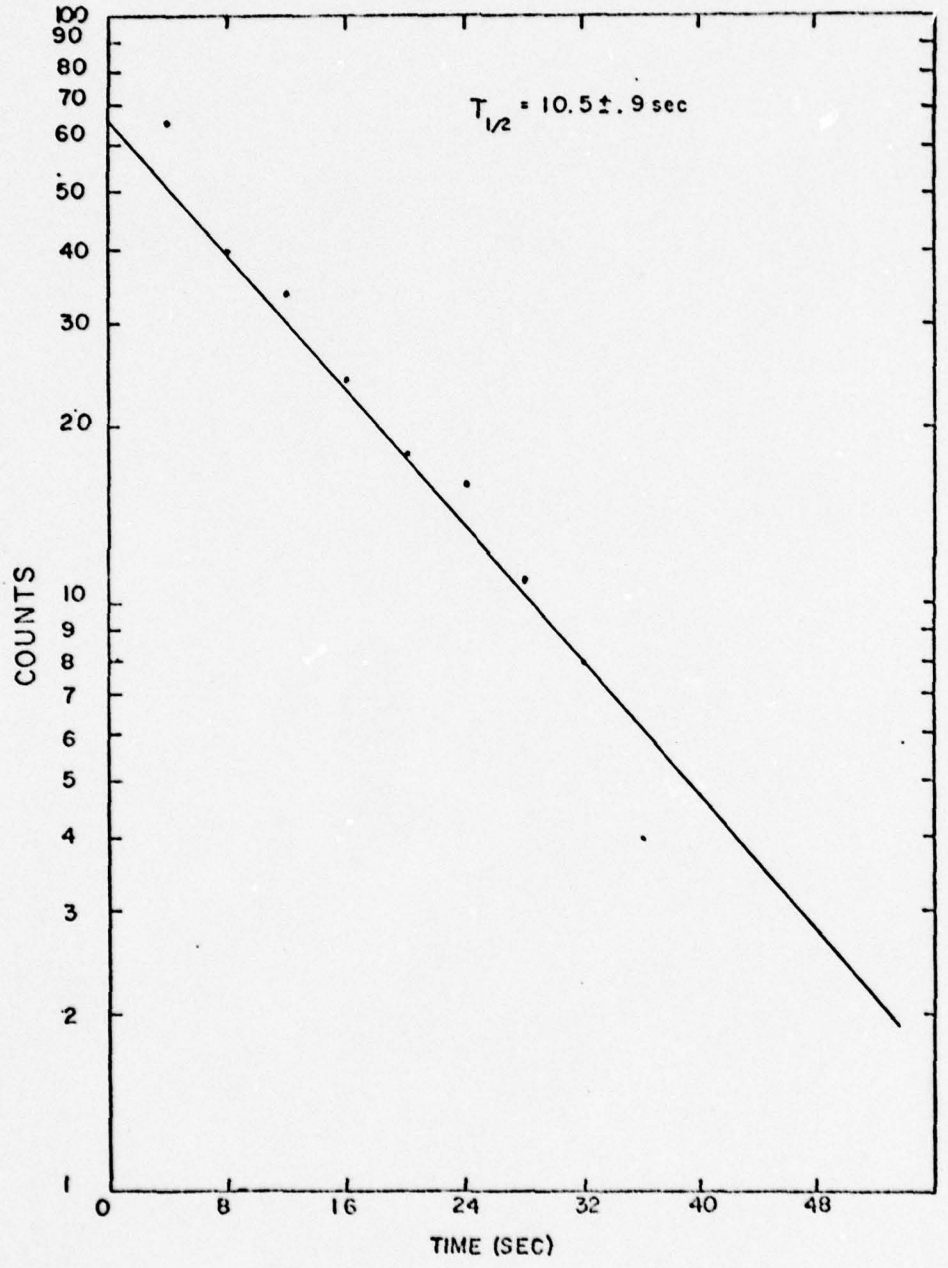
HALFLIFE OF Rn 202
$T_{1/2}$ = 10.5 ± .9 sec
COUNTS
100
90
80
70
60
50
40
30
20
10
9
8
7
6
5
4
3
2
1
0
8
16
24
32
40
48
TIME (SEC)

figure 27

The energy loss through the source is a measured .5 channels, and that through the detector's dead layer, 2 channels. This combined with the intercept value yields the relation:

$$E(MeV) = 1.303 \cdot 10^{-2}(CHANNEL) - .1746$$

Thus, the loss through the detector is 26.1 kV, and that through the source itself 6.5 kV.

As the alphas are formed directly in the detector, a part of the energy of the recoiling nucleus will also be deposited. The relation gives a correspondence between energy and the channel in which that energy was *recorded*; it fails to account for the recoil energy of the nucleus. It is well known that all such energy is not manifested in ionizing collisions. A comparison was made between the known energies of alpha decay and the energies of the channel in which they were recorded. That difference is accounted for if it is assumed that 11% of the nucleus' recoil energy results in ionizations, as shown in Table 1.

Peak integration was performed with the light pen on the Sigma Seven computer at the Tandem facility at BNL, and with cursors on the Heavy Ion group's Prime 300, with which background was subtracted from spectra as well.

Table 2 lists the branching ratios as published in the Nuclear Data Sheets. With these one can account for the

TABLE 1

Parent/ Daughter	D	D	D	P	D	P	P	D	P	P	P	P	P
Channel	479	489	498	501	504	507	514	515	517	524	531	534	544
$E_{CHANNEL}$	6.067	6.197	6.301	6.353	6.393	6.432	6.523	6.536	6.562	6.653	6.744	6.783	6.914
E_{α}	6.057	6.180	6.281	6.345	6.385	6.417	6.500	6.520	6.548	6.636	6.720	6.770	6.910
ΔE	.010	.017	.020	.008	.008	.015	.023	.016	.014	.017	.024	.013	.003
E_{RN}	.121	.123	.125	.126	.127	.128	.130	.130	.131	.132	.134	.135	.138
% Deposited	8.3	14	16	6.3	6.3	12	18	12	11	13	18	9.6	2.2

$\%_D$ = 11%

$\%_P$ = 11%

TABLE 2

Nucleus	State	E_α	%α	Reference
^{200}Rn	0	6910	100	14)
^{201}Rn	0	6720	100	15)
	?	6770	100	
^{202}Rn	0	6636	>70	15)
^{203}Rn	0	6498	66	16)
	310	6548	100	
^{204}Rn	0	6416	72	15)
^{201}At	0	6342	100	15)
^{196}Po	0	6520	100	17)
^{197}Po	0	6281	90	18)
	?	6385	85	
^{198}Po	0	6180	70	19)
^{199}Po	0	5952	88	16)
	310	6059	61	

number of daughter nuclei which decayed by electron capture, and thus determine the number of daughters created by a particular parent. This number should agree quite closely with the number of parental alphas observed. Differences should reflect cross sections of 'daughter' nuclei formed directly from the compound nucleus by particle boiloff.

Figure 28 shows these relative numbers. The curves for 4n and 5n evaporation fit very well. In the case of 5n, one sees that at energies above 181 MeV, the number of daughters exceeds that of parents, indicating a substantial direct formation cross section for ^{198}Po, reaching a maximum in the measured range at 181 MeV of 3.0 mb/sr.

At this same energy, the 6n boiloff daughters are more numerous than parents, but the data is too limited to draw any meaningful conclusions.

The 3n case is of interest since, though the curves are of the same shape, there is an insufficient number of daughters. As seen in Table 2, ^{203}Rn, the parent, has two levels -- the ground state, whose alpha is 6.498 MeV, and a metastable state at 310 keV, the alpha of which is 6.548 MeV. Note also that the branching ratios differ for each state. Both parent alphas were detected, with 23.2% from the ground, and 76.8% from the metastable state.

The daughter, ^{199}Po, also has two alphas, corresponding to two states separated by an energy equal to that which

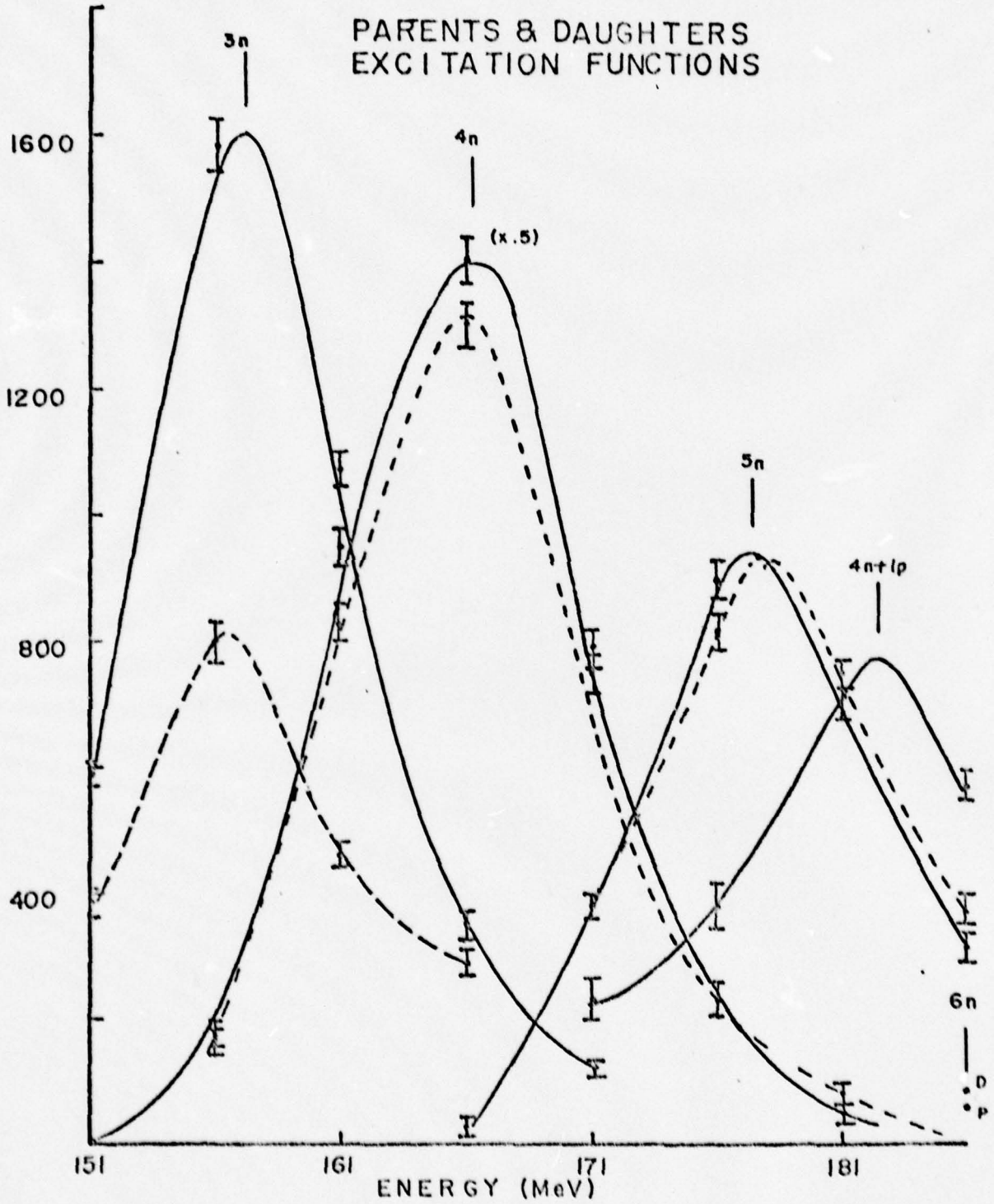
PARENTS & DAUGHTERS
EXCITATION FUNCTIONS
3n
4n
(x.5)
5n
4n+1p
6n
D
P
1600
1200
800
400
151
161
171
181
ENERGY (MeV)

figure 28

separates its parent's. If one assumes that the decays of the parent will be to the corresponding state in the daughter, then it is expected that the relative numbers of each type should be preserved. Unfortunately, the 5.952 MeV ground state alpha from ^{199}Po cannot be detected, being hidden in the beam tail. The other alpha, the 6.059 MeV, was detected; and by extrapolation, the expected number of ground state alphas was determined. These numbers were corrected for electron capture branching and summed, yielding the daughter values of fig. 28.

The discrepancy cannot be explained away by proposing that gamma transitions from the metastable state to the ground might have increased the relative number of 'lost' alphas, and invalidating the extrapolation used. The decay constant for this E5 transition is so small that the nucleus will have alpha decayed long before the transition could take place. Hence, the observed branching ratio of 38% is in disagreement with the accepted value of 61% for ^{199}Po.

Because the range of the alpha particles emitted in the detector is about 5.6 times that of its parent compound nucleus, one expects only 55.7% of these alphas to fully deposit their energy based on this geometry. The fusion gates, corrected for this geometrical effect, can be compared to parent alphas, corrected for electron capture, as in fig. 29. Any direct daughter formation should be reflected

EXCITATION FUNCTION

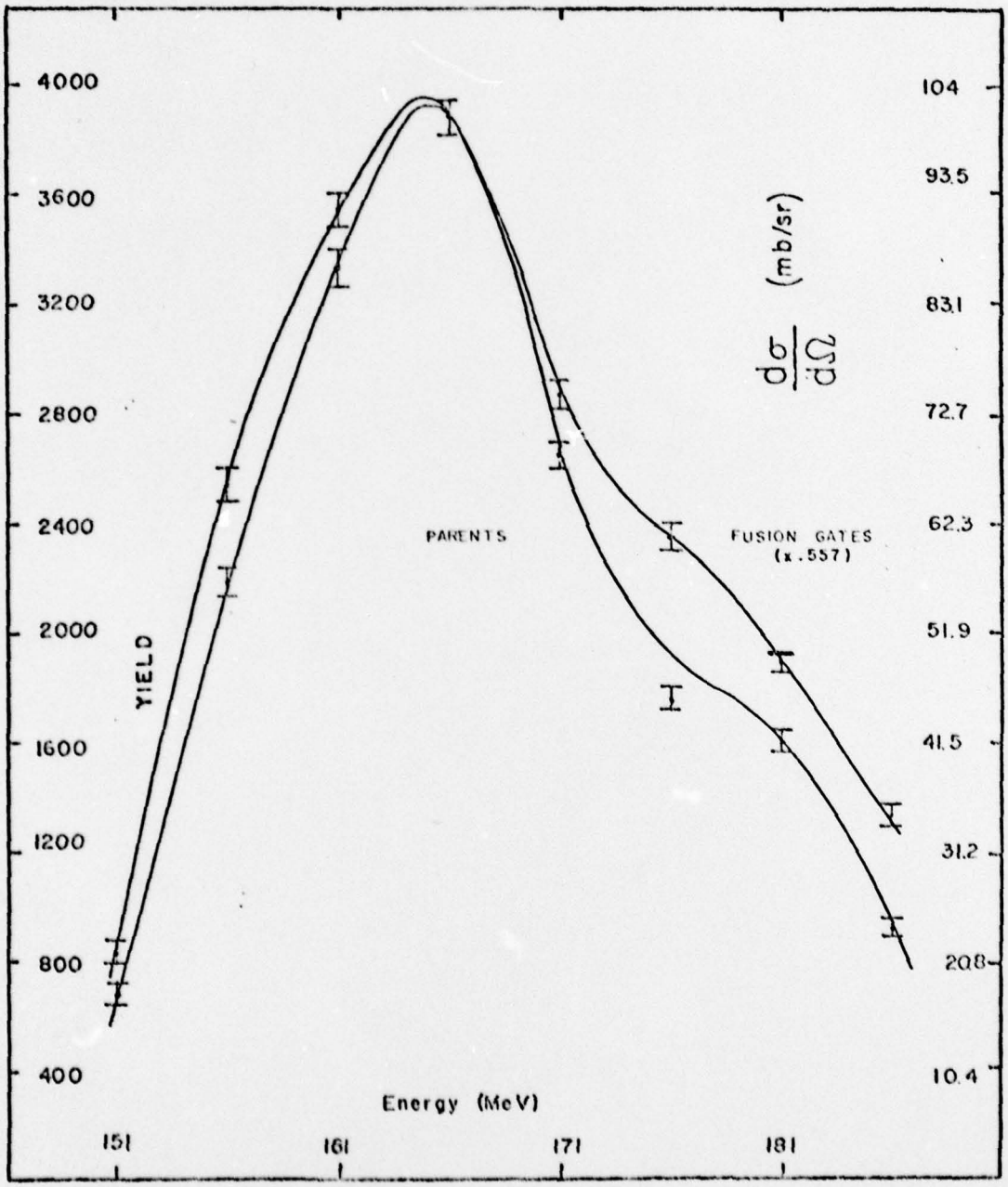

figure 29

in the difference between fusion gates and alphas. The agreement is close up to about 176 MeV, where "daughters," particularly ^{197}Po, are formed directly.

To determine the evaporation residue differential cross section from the results, the fact that the scattered particles in the monitors are purely Rutherford is made use of, so

$$\frac{d\sigma_{ER}}{d\Omega} = \frac{N_{ER}}{N_{MON}} \frac{\Delta\Omega_{MON}}{\Delta\Omega_{ER}} \frac{d\sigma_{RUTH}}{d\Omega}$$

where N is counts, $\Delta\Omega$ is solid angle, and $\frac{d\sigma_{RUTH}}{d\Omega}$ is the Rutherford scattering cross section, which is readily calculated to be 14.06 barns/steradian for the beam, target, energy, and geometries under consideration. The counts are measured directly and $\Delta\Omega_{RUTH}$ is simply the combined solid angles of the monitors. Yet, from fig. 16 these monitors give an energy spectrum integrated over velocity.

The velocity selector, however, analyzes vertically based on velocity, and thus the acceptance solid angle is very much dependent on the velocity distribution of the incoming particles. Using Raytrace calculations, the solid angle dependence on this distribution was determined, as shown in fig. 3. The curve may be roughly approximated by a gaussian with $\sigma = 3.9$, and a mean of 1.2. Since the velocity selector convolutes velocity with direction of

emission from the target. We measure:

$$\int_{-\infty}^{+\infty} f(v)\Omega(v-v_o)dv = F(v_o)$$

$f(v)$ is the true velocity distribution, $\Omega(v-v_o)$ is the velocity dependent solid angle, and $F(v_o)$ is the measured velocity distribution. If we assume the true distribution is gaussian, its σ may be found by subtracting in quadrature σ of the solid angle function from that of the measured profile, giving a value $\sigma = 3.0$. Convoluting this with the solid angle function results in the determination that our velocity integrated solid angle was only 76.5% of $\lim_{\Delta v \to \infty} \int_{v_o-\Delta v}^{v_o+\Delta v} \frac{\partial \Omega}{\partial v} (v-v_o)dv$. Hence, the augmented solid angle value must be used in the cross section calculation, giving a differential cross section of 44.8 mb/sr.

A correction is made to account for residues stopped by the baffles, which were used to reduce the inherent background, by multiplying by the fractional count rate with the baffles removed, giving: 60.8 mb/sr.

From fig. 29 it is readily noted that this cross section peaks not at 175 MeV at which it was measured, but rather at 166 MeV. Scaling by relative count rates, we determine

$$\frac{d\sigma}{d\Omega}ER = 101.4 \text{ mb/sr} \qquad \text{at } 166 \text{ MeV}.$$

The total fusion cross section if found by integrating this value over solid angle. For our small value of σ in the angular distribution, we may integrate by appealing to

$$\sigma_T = 2\pi\sigma^2 \, Ym$$

from which we arrive at the result of 1.09 mb, at 166 MeV.

CHAPTER IV

GOLD EXPERIMENT

With the results of the thulium experiment offering convincing evidence that the apparatus was working properly, with effective elimination of the beam tail and good focusing onto the detector, a search for the evaporation residues from the gold was conducted. An energy close to the Coulomb barrier was selected as to offer the possibility for fusion, without an excessively great deal of excitation energy in the compound nucleus. With that consideration, 179 MeV was chosen. A calculation similar to that for the case of ^{169}Tm was made to determine the velocity selector and quadrupole field settings of 45.5 kV and 3.88 kG, and 1.52, respectively. The small 0.06 kG field on the dipole was retained to vertically center the focus.

The target was a self supporting, 500 micrograms/cm^2 gold foil. The 600 mm^2 solid state detector was used. Figure 19 shows the electronics. The description of this set up is the same as that for the run with thulium, except that the multiscalar automatic reset occurred after only 10 sec after detection of a possible evaporation residue, in keeping with the expected short lifetimes.

The result of seven hours of running under these conditions was the appearance of 243 particles of the correct

energy to be gated by the TSCA. A possible alpha from only one of these, however, was detected. This candidate had an energy of 5.9 MeV and appeared in time channel zero. With only one such count, it is impossible to assert that it, in fact, was an alpha particle, the other 242 counts being thulium knock-outs.

If it were an alpha, an upper limit in the fusion cross section can be readily established. Assuming the same solid angle of acceptance function as in the thulium experiment, the differential cross section is determined to be:

$$\frac{d\sigma}{d\Omega} \text{ ER} = 4.06 \text{ microbarns/sr}$$

If the same angular distribution for the evaporation residues of thulium is assumed for gold, the total cross section is 60 nanobarns, with the correction for the baffles included.

CHAPTER V

COMPARISON WITH THEORY

The statistical theory of Weisskopf and Ewing[20] best serves to describe the de-excitation of a compound nucleus through particle evaporation. The relation:

$$\rho_\nu(\varepsilon)d\varepsilon = \frac{(2s+1)_\nu \mu_\nu \varepsilon \sigma_\nu(\varepsilon)\rho(E_f)d\varepsilon}{\sum_{\nu=1}^{n}(2s+1)_\nu \mu_\nu \int_0^\infty \varepsilon\sigma_\nu(\varepsilon)\rho(E_f)d\varepsilon}$$

gives the probability of emission of a particle ν with energy between ε and $\varepsilon+d\varepsilon$, spin s, reduced mass μ, and inverse cross section $\sigma(\varepsilon)$ from an excited nucleus to form a nucleus of level density $\rho(E_f)$. This density may be approximated by the Fermi gas level density, $\rho(E, J=0) \propto E^{-2}\exp 2\sqrt{aE}$, where a is the nuclear level density parameter, taken to be about A/10 MeV^{-1}. It is assumed that $\rho(E,J)=(2J+1)\rho(E,J=0)$.

The nuclear evaporation code ALICE[21] is capable of performing the above calculations for each possible step of the evaporation cascade, and hence predict the cross section for the eventual nuclides. It also calculates total reaction cross sections from the parabolic model, inverse reaction cross sections using the optical model, and fusion competition using the rotating liquid drop model.[22]

The program was run for the ^{169}Tm reaction at the

same energies as those used to determine the excitation functions. The results are shown in Table 3, along with the relative experimental abundances.

The ALICE calculation indicates very low cross sections for the lower energies used, and anomalous relative cross sections, with ^{198}Po being the most favored predicted product, while barely a trace was observed directly at the highest energies.

Since ALICE does not allow for the diffuseness of nuclear shape, it was altered to permit variation of the radius as an input parameter. The barrier factor was set at different values to observe the effect of reducing or increasing fission competition. The critical partial wave was found using the experimentally determined value of the compound nucleus formation cross section. Since it is widely held that the lowest values of angular momentum go into formation of the compound nucleus, and high values into fission, the value of $\ell = 1$ was chosen since, at 176 MeV, to it corresponds a total cross section of 0.599 mb, compared to an experimental value of 0.654 mb. Both JANG options were used; =1 removes one unit of angular momentum for a nucleon and ten for an alpha; =0 does not remove angular momentum.

ALICE calculates level densities using excitation energies that include the rotational energy, and does not use the residue's mass in determining the density parameter 'a'.

A correction for this latter shortcoming was applied, as shown in Table 3.

It is clear that the predicted abundances differ considerably from those determined experimentally. Species produced by the emission of a proton or an alpha particle are quite favored theoretically; yet, the experiment failed to produce any ^{198}Po at 176 MeV, and ^{201}At was present but in an amount considerably less than was predicted.

The emission of an alpha particle gives the nucleus a considerably larger impulse than that of a nucleon, and would consequently broaden the angular distribution and velocity profile, depending on the direction of emission, and hence attenuate the cross section of the residue thus formed relative to others. But it should not be diminished to zero. Also, the excitation function of 4n,α should not be expected to have the same shape as that of 4n, yet from fig. 28 it is seen that the parent and daughter are quite closely matched. It must be concluded that ^{198}Po is simply not formed through 4n,α emission.

The results indicate a clear limitation as to the applicability of the ALICE code to reactions of this type, the emission of protons, and especially alpha particles, being greatly exaggerated.

TABLE 3

RELATIVE ABUNDANCES OF EVAPORATION RESIDUES AT 176 MeV

Species	Exp Abundances	R_o= 1.22 BF= 0.65 JANG= 1	1.30 0.60 1	1.30 0.60 0	1.30 0.9 1	1.30 0.9 0	level density correction
^{202}Rn	32.0%	0.5	0.7	0.8	1.6	1.6	2.3
^{201}Rn	46.5	2.3	4.4	5.2	15.1	15.8	18.7
^{201}At	21.4	23.0	33.4	34.4	42.2	41.8	49.2
^{198}Po	0	74.2	61.5	59.6	41.1	40.7	29.9

CHAPTER VI

CONCLUSIONS

These experiments offered impressive evidence that the newly installed apparatus is decidedly effective in meeting its design criteria, that of detecting evaporation residues from low yield reactions, and doing so at 0°. As explained earlier, meeting these two conditions is necessary for studying reactions that may produce superheavies via heavy ion fusion.

The method of determining half lives of decaying species also proved effective, confirming the accepted half life of ^{202}Rn.

The disputed branching ratio for ^{199}Po should be further investigated. An out-of-beam spectrum would reveal the actual number of 5.952 MeV alphas, those that were 'lost' in the beam tail in this experiment, so that a more confident determination of the branching ratio can be made.

Conclusions about null experiments are difficult. An upper limit of 60 nanobarns is quite low, disappointingly so. Longer runs are required to support or refute this estimate. The minuteness of the cross section provides, unhappily, no new information as to the reaction mechanisms involved in heavy ion fusion reactions.

ACKNOWLEDGEMENTS

I would first like to thank my thesis advisor, Professor Harald A. Enge, for his support and direction throughout this project.

As this thesis is by no means the result of an individual effort, I wish to express my appreciation to those who shared in the task.

John Molitoris lent his energy and enthusiasm during the many runs; Dr. W. Schier provided leadership and insight; Dr. Glenn Young shared his extensive knowledge of electronics; Anthony Sperduto handled and scanned the lexan plates; Tony Luongo made targets; Ed Druek restored the magnets and kept everything working; Matti Salomaa helped out on all runs; Henry Sang and Bill Thoms assisted with the graphics contained herein; and Ms. Carol Tinelli, along with giving me much appreciated encouragement, did a masterful job in typing this draft.

Dr. Joe Chervenak deserves a special thanks. He provided a steady pace over the many miles we ran together, provocative topics for discussion on midnight shifts at BNL, an enormous amount of Raytrace output, and helpful answers to my myriad questions. I value my association with him greatly.

REFERENCES

1) C. Bemis and J. Nix, Comments on Nuclear and Particle Physics, Vol. 7, 3 (1977) 65-78.

2) G. Seaborg, Ann. Rev. Nucl., 18 (1968) 56.

3) R. Beringer, Phys. Rev. Letters, 18 (1967) 1006-7.

4) D. Horn et al., Phys. Rev. C, Vol. 17, 1 (1978) 118-125.

5) C. Bolton, W.A. Schier, N. Tsoupas, H. Enge (unpublished).

6) W. Schier (unpublished).

7) M. Salomaa and H. Enge, Nucl. Instr. & Meth., 145 (1977) 271-277.

8) H. Enge, D. Horn, Nucl. Instr. & Meth., 145 (1977) 277-282.

9) H. Enge, Rev. Sci. Instr., 35 (1964) 278.

10) H. Enge, Rev. Sci. Instr., 30 (1959) 248.

11) H. Wegner (unpublished).

12) Betz, Rev. Mod. Phys., 44 (1972) 505ff.

13) P. Bevington, Data Reduction and Error Analysis for the Physical Sciences (McGraw-Hill, N.Y., 1969).

14) Nucl. Data Sheets, B6 (1971) 387.

15) Nucl. Data Sheets, B5 (1971) 561.

16) Nucl. Data Sheets, 2411 (1978) 167.

17) Nucl. Data Sheets, B7 (1972) 395.

18) Nucl. Data Sheets, 2012 (1977) 108.

19) Nucl. Data Sheets, 2011 (1977) 377.

20) V.F. Weisskopf and D.H. Ewing, Phys. Rev. 57 (1940) 472.

21) M. Blann and F. Plasil, ALICE, U.S. Atomic Energy Commission Report No. COO-3494-10, 1973 (unpublished).

22) D. Horn, Heavy Ion Reactions With Proton Rich Nuclei (Ph.D. Thesis, M.I.T., August 1976).